12-2014

Transformation of Uranium in a Geological Environment

Derrell Hood
Clemson University, derrelh@g.clemson.edu

TRANSFORMATION OF URANIUM IN A GEOLOGICAL ENVIRONMENT

A Thesis
Presented to
the Graduate School of
Clemson University

In Partial Fulfillment
of the Requirements for the Degree
Master of Science
Environmental Engineering

by
Derrell Hood
December 2014

Accepted by:
Lindsay Shuller-Nickles, Committee Chair
Tim Devol
Brian Powell

ABSTRACT

Incorporation of uranium into iron oxide minerals is a promising mechanism for the environmental immobilization of U(VI). In this study, synthesized hematite was doped with uranium and analyzed with SEM-EDS, TEM, XRD, and ICP-MS. The results of this analysis strongly indicate uranium incorporation into the mineral, as well as the possible presence of a co-precipitated uranium mineral clarkeite. Preliminary results also shows an increase in the amount of uranium associated with the hematite particles as a function of mineral aging.

Cyclic Voltammetry (CV) was used to induce and characterize electrochemical changes of uranium in the doped hematite system; these changes may possibly affect the stability of the bulk hematite, as well as the solubility of incorporated uranium should the hematite dissolve. The latter scenario is of particular interest, given the possibility of corrosive pH and temperature conditions in a geological waste repository. For this reason, uranium redox reactions were investigated at varying physical conditions. CV experiments demonstrated that a rapid and reversible U(V)-U(VI) redox couple will form in the presence of an applied cyclical voltage. The redox reactions between U(IV) and U(VI) are also possible, but are kinetically slower. All uranium redox reactions were most strongly observed in a narrow pH range centered around pH 3.5. The rate of each redox reaction increased with increasing temperature, while the electrochemical potential decreased with increasing temperature. These results are the groundwork upon which to conduct additional testing to further assess the viability of uranium incorporation as a strategy for uranium waste sequestration.

DEDICATION

To my late father, Rodger Hood. Though I wish I could have shared my Clemson journey with him, I am thankful for the legacy and example he left behind. If I can live a life that models his dedication to family, ███ and to professional excellence, I will have considered it well-lived indeed.

ACKNOWLEDGMENTS

I would like to acknowledge my advisor, Dr. Lindsay Shuller-Nickles, for the innumerable ways she has assisted me in my journey at Clemson. It is fair to say that I would not have attended Clemson if not for her encouragement to pursue my studies here, and the opportunity she provided to do so. She has also been incredibly supportive of my career aspirations and the resulting unconventional academic path I was required to follow during my graduate studies. I could not have asked for a better advisor to guide and assist me through my Clemson journey.

I would also like to thank my family for their daily encouragement and support. Though separated by distance, they were never far away. I am incredibly grateful for their support and assistance throughout my studies.

TABLE OF CONTENTS

Table of Contents (Continued) Page

LIST OF TABLES

LIST OF FIGURES

CHAPTER ONE

Introduction

Nuclear energy is uniquely positioned to reduce both carbon emissions[1] and global dependence on non-renewable fossil fuel resources, and will thus likely remain a key component of future energy policy. Nuclear power is operationally less dependent on local climate and geography than other potential energy alternatives, and its ability to generate power with low land, fuel, and emission footprints allows nuclear power to fulfill a primary role on the energy grid. If coupled to increased efficiencies in mineral extraction and reactor design that increase the total energy extraction from uranium ore reserves, known nuclear resources hold the potential to fulfill global energy needs for many decades to come.[2]

Yet, the single greatest issue currently facing the nuclear industry is that of waste disposal. Waste is generated at all points of the nuclear fuel cycle and has varying chemical properties and radioactivity. In the commercial nuclear industry, spent nuclear fuel (SNF) has the highest activity to volume ratio and requires the longest period of sequestration due to the presence of actinides, actinide daughters, ^{129}I, and ^{99}Tc. If and when a permanent repository for domestic SNF is selected, the local geology, chemistry, climate, and other factors must be thoroughly studied to anticipate the likely environmental fate of the disposed radionuclides. The time scales of concern for long term disposal are on the order of geological time, *i.e.*, hundreds of thousands of years, making long-lived radionuclides the waste substance of greatest environmental concern.

It must be assumed that the release of radionuclides from the source term will eventually occur due to corrosion of engineered barriers. Upon break-down of the engineered barriers and waste form, aqueous transport of actinides is possible. Previous fundamental research has primarily focused on the chemical fate of radionuclides released from the corrosion of SNF[3,4,5]. In these studies the properties of uranium is of particular importance since it comprises 95% of SNF[6].

Perhaps the most important aspect of this research is the study of how aqueous uranium may be immobilized. Although the specific mechanisms can be quite complex, they may be broadly classified into three main groups: sorption, reduction and precipitation on the mineral surface, and direct incorporation into proximal minerals. Fundamental research into each of these processes is necessary to better understand specific mechanisms and the influence of environmental parameters, such as pH and ionic strength, on those mechanisms. This knowledge can then be applied to de-convolute the complex interaction of site-specific environmental characteristics on uranium immobilization. Greater confidence in the capability of a given disposal site to safe-guard the public from actinide exposure can then be attained.

CHAPTER TWO

Background

Environmental Speciation of Uranium

In the environment, uranium occurs primarily in one of two oxidation states: U(IV) and U(VI). U(IV) generally forms insoluble compounds (*e.g.*, uraninite UO_2), while U(VI) is the dominant aqueous oxidation state under a wide range of environmental conditions[3] and forms the uranyl dioxycation (UO_2^{2+}). Uranyl readily complexes with ligands and, as a hard acid, shows particular affinity for hard base ligands, such as hydroxide and carbonate[6]. Many of these ligands are ubiquitous in geological formations favored for nuclear waste disposal. The concentration of these ligands is highly dependent on local geochemical conditions and resultant pH. As a result, site specific data should always be used for accurate modeling. The natural pH range of groundwater ranges between 5-9, with an average value slightly above 7[7].

Uranium in SNF is initially stored in engineered waste canisters, which provide isolation from groundwater. However, over geological time, it can be assumed that corrosion and radiation damage will eventually degrade the canisters and allow the uranium to become exposed to groundwater. In the presence of water, radiolysis of water at the surface of the used nuclear fuel causes oxidizing conditions which favor U(VI) speciation[8]. As a result, the potential for release of uranyl from nuclear waste forms is a critically important risk driver for many repository sites.

Immobilization of Aqueous Uranium

Several mechanisms may impede the mobilization of aqueous uranium, including sorption and reduction onto mineral surfaces, precipitation of insoluble phases, and incorporation into proximal minerals. Aqueous uranyl complexes can form inner-sphere complexes at mineral surfaces or as outer-sphere complexes[9]. Outer-sphere complexes are characterized by long-range electrostatic interactions in which uranyl is separated from the mineral surface by a layer of water molecules. Inner-sphere complexes involve chemical bonding at the mineral surface and can, therefore, comprise a strong immobilization mechanism, if the reaction is irreversible. The sorption strength of uranium ions is based on the effective charge of the uranium ions and given by the following series:

$$U^{4+} > UO_2^{2+} \sim U^{3+} > UO_2^{+}$$
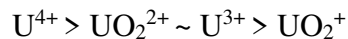
where U(IV) will sorb most strongly. In this series U(VI) and U(V) occur as uranyl molecules, which is their predominant environmental form.

U(VI) sorption is often accompanied by the reduction of U(VI) to U(IV) via interaction between U(VI) and reducing agents such as Fe(II)[10]. Because U(IV) forms primarily insoluble species, uranium immobilization is enhanced due to increased U(IV) speciation. The bonding of actinides in inner sphere sorption is primarily ionic in nature[9]. Environmental changes that affect electrostatic interactions in the source term may in turn lead to desorption and subsequent release of uranium from a mineral surface. Common examples of such electrostatic alterations are changes in pH or ionic strength. Sorption

may retard the aqueous transport of soluble U(VI) complexes, but it cannot be viewed as a permanent immobilization mechanism and may even enhance transport in the case of sorption to colloidal particles[11,12].

If the kinetics of sorption are favorable, sufficient amounts of U(VI) may sorb to the surface to allow for surface mediated precipitation of solid U(VI) phases. If the concentration of U(VI) is well above the solubility limit, precipitation of U(VI)-bearing minerals may be viewed as a more permanent immobilization mechanism relative to sorption/reduction. Given the prospect of aqueous uranium leaching from a waste form, a method that preferentially sequesters the most soluble form of uranium for indefinite periods of time is highly desirable. An intriguing possibility with regards to irreversible environmental sequestration of uranium is incorporation into proximal mineral phases, where U(VI) occupies a lattice or interstitial site within a mineral. The degree to which incorporation into proximal mineral phases immobilizes the uranium is a key question in determining the efficacy of a repository. If it can be shown that, upon release, U(VI) is readily immobilized, the risk of ultimate release and human exposure is greatly reduced. For example, in oxidizing conditions uranium incorporation into iron oxides has been shown to limit the release of uranium as soluble U(VI)[13].

Uranium and Iron Mineralogy

Predicting the theoretical viability of uranium incorporation into a proximal mineral requires two key considerations: (*i*) the net charge for the substitution must remain neutral and (*ii*) the coordination environment of the mineral must be consistent

5

with known uranium coordination environments. Therefore, an evaluation of uranium mineralogy with a focus on coordination environments is a necessary first step towards predicting incorporation into proximal minerals. Since U(IV) is not a significant risk driver for aqueous transport, only U(VI) mineral chemistry will be briefly considered.

As previously mentioned, U(VI) forms the linear uranyl moiety (UO_2^{2+}), which is typically coordinated by four to six ligands, forming square, pentagonal, and hexagonal bipyramids[14,15]. The uranyl bipyramids typically polymerize to form sheet structures, which account for 204 of 368 identified uranyl minerals[15]. In some instances, the uranyl bipyramids form framework structures. Interestingly, two known framework structures, ($Pb_2(H_2O)[(UO_2)_{10}UO_{12}(OH)_6(H_2O)_6]$) and ($NH_4)_3(H_2O_2)\{[(UO_2)_{10}O_{10}(OH)][(UO_4)(H_2O)_2]\}$, include uranyl bipyramids, as well as distorted U(VI) octahedra[15]. This observation is important, because Fe(III) is also octahedrally coordinated in several common iron oxide minerals (e.g., goethite FeOOH and hematite Fe_2O_3). As a result, these structures indicate that U(VI) substitution into an Fe(III) mineral may be possible. While the distorted U(VI) octahedra do not dominate the structures mentioned above, (*e.g.*, 1/6 of all U(VI) are octahedrally coordinated in $Pb_2(H_2O)[(UO_2)_{10}UO_{12}(OH)_6(H_2O)_6])$[15], the octahedral coordination indicates that U(VI) may be incorporated into octahedral sites of other minerals such as hematite (Fe_2O_3). Moreover, Ba_2MgUO_6 and $K_9BiU_6O_{24}$ are examples of framework structures composed of octahedrally coordinated U(VI) cations with no uranyl ions present[15]. These structures provide further evidence of possible U(VI) substitution into an octahedral site.

Iron oxide minerals are environmentally ubiquitous, readily sorb uranium, and often participate in Fe(II)-mediated uranium reduction/co-precipitation reactions. Hematite (α-Fe_2O_3) is among the most common forms of iron oxide and is an important constituent in many geological environments. In addition, hematite is expected to form as a high temperature corrosion product of stainless steel waste canisters[16]. Hematite contains octahedrally-coordinated Fe(III). The mineral structure is described as parallel layers of octahedra in which two thirds of the octahedral sites are filled with Fe(III)[17]. Substitution of one U(VI) ion for two Fe(III) ions satisfies charge balance. In addition, the ionic radii of octahedrally-coordinated U(VI) and Fe(III) differ by 11%. Thus, Pauling's Rules state that they may substitute for one another. (<10%, if < 15% than they may substitute with limited solubility)[18].

Incorporated U(VI) is not soluble in an aqueous environment due to the coordination environment of the bulk mineral. However, reduction of incorporated U(VI) may alter coordination polyhedra and effect the thermodynamic stability of the U-incorporated mineral. Unfortunately, assessing the theoretical possibility of such electrochemical changes is difficult. Uraninite, the dominant U(IV) mineral, has the fluorite structure (*Fm3m*), where U is octahedrally coordinated. Therefore, reduction of octahedrally incorporated U(VI) to U(IV) may be possible without destabilizing the mineral structure. U(IV) has an ionic radius of 0.89 Å (37% larger than the ionic radius of Fe(III)), and thus steric hindrances may be a concern in the event of such a redox transformation.

Evidence for Uranium Incorporation into Iron Oxide Minerals

U(VI) has been shown to directly substitute into a variety of iron hydroxide minerals. For example, uranium incorporation into two-line ferrihydrate has been identified[18]. Two-line ferrihydrate is structurally distinct from more common iron oxides such as hematite, yet retains many similarities in terms of the observed iron coordination environment and possible uranium substitution mechanisms. Two-line ferrihydrate is characterized by layers of edge-shared FeO_6 octahedra (known as Fe1 sites) that are connected vertically by FeO_6 octahedra (known as Fe2 sites). The Fe2 sites share edges with Fe1 sites and FeO_4 tetrahedra (Fe3 sites). The Fe1 sites are completely filled, whereas the Fe2 and Fe3 sites retain ~50% vacancies. However, the direct substitution of U(VI) for Fe(III) results in a charge imbalance. A variety of potential mechanisms could address this charge imbalance, such as coupled removal of Fe from an adjacent Fe1 site. The potential for uranium substitution into disordered ferrihydrate is significant given the fact that aging transforms ferrihydrate into highly ordered crystalline structures. Increased ordering corresponds to additional octahedral sites, which are more likely to incorporate uranium and limit its mobility[19].

Additional studies imply the potential for U(VI) incorporation into Fe(III) hydroxides (goethite) as a function of increasing amounts of U(VI) that could not be recovered from the liquid phase during synthesis experiments[20,21]. This observation strongly indicated that U(VI) was becoming fixed within the solid mineral phase. A method was then developed to fix uranium within a solid iron oxide (hematite) mineral phase[22]. Recent X-ray absorption fine structure (XAFS), X-ray absorption near edge

structure (XANES), and Fourier transform infrared (FT-IR) structural data provided compelling evidence for the incorporation of uranium into the hematite crystal structure[23]. Reduction experiments conducted after synthesizing U-doped hematite showed a much higher population of U(V) relative to U(IV)[23]. This observation is in contrast to the speciation of adsorbed uranium, in which U(IV) and U(VI) predominate. Therefore, the prevalence of U(V) was likely due to the relative stability of the ion in an octahedral environment relative to adsorbed U(IV). These findings indicate that uranium can be incorporated into the hematite structure via substitution into an octahedral coordination environment. The exact mechanism of the substitution is not yet known. Nevertheless, the experimental verification of incorporation is significant due to its possible use as a mechanism for limiting the mobility of uranium in the environment. As previously stated, incorporated U(VI) can only be released to the aqueous phase via alteration of the bulk mineral phase.

From an environmental standpoint, it is unlikely that uranium incorporation into a mineral phase will be accomplished without some adsorption to the mineral surface, as well. Even in the case of relatively complete incorporation, some uranium will likely remain on the surface of the mineral and be effectively sorbed. In this case, surface adsorption becomes the primary source of aqueous uranium due to the greater reversibility of the process. Changes in environmental parameters such as temperature and pH are more likely to cause uranium desorption from the mineral surface prior to degradation of the mineral structure.   Therefore, the effect of environmental parameters

on uranium sorption strength to the mineral surface should be considered in any disposal scenario.

It has been shown that uranium reduction is strongly influenced by the Fe(II)/Fe(III) redox couple at a mineral surface[24], where the stoichiometric ratio of Fe(II) to Fe(III) determines the extent of U(VI) reduction. At standard conditions in aqueous solution, the reduction potential of Fe(III) is 0.771 V, while that of U(VI) to U(IV) is 0.273 V[25]. Assuming similar reduction potentials for hematite with incorporated uranium, these values indicate that iron is more readily reduced than uranium. However, the positive potential for both uranium and iron indicate that both ions are readily reduced in the presence of a reducing agent.

For incorporated uranium, reduction to U(V) is energetically favorable relative to U(IV)[23]. Disproportionation of U(V) may be more thermodynamically favorable in some cases and allow for an alternative pathway for the formation of U(IV). Disproportionation of U(V) is an important electrochemical mechanism that has been demonstrated in a variety of geologic and biologic environments[26]. For uranium sorbed on the surface of iron oxide minerals, U(V) is considered to be a fleeting intermediate due to the rapid kinetics of the disproportionation reaction. In the case of structural incorporation, the thermodynamic favorability of the U(VI) to U(V) reduction may favor speciation of U(V) relative to U(IV) in a reducing environment[23]. However, the long term stability of U(V) within the mineral has not yet been confirmed. Since disproportionation is an important mechanism for sorbed U(V) redox, it must also be

considered as a possible mechanism when assessing the long term speciation of

incorporate uranium.

In addition to disproportionation, pH also affects uranium speciation in aqueous

systems, and thus impacts solubility and sorption onto surfaces. Acidic conditions

encourage the oxidation of U(V) to U(VI), whereas at highly basic pH's of ~13, U(V)

and (VI) easily form a precipitate surface layer on iron (hydr)-oxide surfaces[27]. It should

be noted that pH is also a key factor in aqueous uranium speciation due to pH-mediated

effects on hydrolysis reactions[18]. Sorption isotherms indicate that uranium sorption

progressively decreases at low pH due to electrostatic repulsion at the mineral surface,

and vice versa at high pH. Regardless of ionic speciation, uranium that is not part of a

solid co-precipitated phase will therefore become more soluble with decreasing pH. (See

Figure A.1)

Fundamental Electrochemical Relationships

The basic relationship that determines the potential of an electrochemical reaction

is given by the Nernst equation:

$$E = E° - \frac{RT}{nF} * \ln Q \tag{1}$$

Where T is the temperature, R is the gas constant (8.3145 J/mol∘K), E° is the standard

cell potential, n is the stoichiometric number of electrons transferred, F is the Faraday

constant (9.648 x 10^4 C/mol), and Q is the reaction quotient. In aqueous systems, Q is

often pH dependent. For example, in carbonate free systems uranyl is found as

$UO_2(OH)_x$, where pH determines the number of hydroxide groups associated with the uranyl ion.

The electrochemical potential of a redox process deviates from its standard potential as the temperature, concentration of reactants, and pH changes. Therefore, the electrochemical potential is strongly dependent on ambient physical conditions. The relationship between electrochemical potential and Gibbs free energy (ΔG) is given as follows:

$$\Delta G = -nFE \tag{2}$$

Since Gibbs free energy is a direct function of electrochemical potential, temperature and pH are expected to have an effect on the thermodynamic favorability of uranium redox processes in doped hematite.

Using Cyclic Voltammetry to Probe Geochemical Reactions

Voltammetric methods are a type of electrochemical method that have proven useful in characterizing redox sensitive minerals such as Fe sulfide minerals (*e.g.*, pyrite FeS_2[28]) and Fe oxide minerals (*e.g.*, magnetite Fe_3O_4).For example, one of the earliest known applications of voltammetry determined the reduction potential of cadmium[29]. In addition, voltammetry has been used to obtain rate constants and half cell potentials for uranium redox reactions in solution[30]. The electrochemical behavior of uranium sorbed onto hematite, goethite, and other iron oxide minerals has also been investigated using voltammetry[31].

Each ionic species has a quantifiable potential energy that corresponds to the thermodynamic favorability of either oxidation or reduction. For a redox reaction to occur, an applied voltage must supply the minimum energy required for oxidation/reduction. If a constant voltage is applied to a sample, the equilibrium of the ionic species will be disturbed. To re-establish equilibrium either oxidation or reduction will occur, which in turn generates a current (*i.e.*, a flow of electrons). The magnitude of the current depends on the ionic concentration, temperature, and the equilibrium constant of the redox system at a given set of conditions. Thus, the total current generated by an applied voltage is a function of the physical and chemical characteristics of the system.

Voltammetric methods use the application of a changing voltage, normally at a fixed rate versus time. The analyte may undergo multiple redox transformations as potentials are progressively reached, which correspond to the energy requirements of the redox reaction. As electrochemical reactions occur, total current varies with time. Linear sweep voltammetry is a method that applies a linearly changing voltage from a chosen starting potential. As potentials are reached that are sufficient to induce redox reactions, a spike in current is observed as the species is initially oxidized/reduced. If the terminal potential (*i.e.*, the voltage at the positive or negative of the chosen potential range) is sufficiently high, complete oxidation may occur if the reaction kinetics are favorable during the experimental time scale. Some electrochemical changes may be reversible and/or correspond to an equilibrium between multiple oxidation states. While useful for the qualitative identification of peak onsets, linear sweep voltammetry does not allow for equilibrium characterization of redox systems.

Cyclic voltammetry (CV), unlike linear sweep voltammetry, allows the application of a voltage to continually oscillate between a high and low value. As a result, oxidation and reduction reactions can be reversibly induced in the same experiment. Observed increases in current can be attributed to a specific redox reaction, which in turn allows additional kinetic and thermodynamic information to be attained. CV was selected as the primary method to accomplish the experimental goals of this research for two main reasons: (1) it allows redox couples to be induced in a single experiment and (2) it yields kinetic and thermodynamic information for each redox reaction.

In a CV experiment, the scan rate, step interval, upper/lower switching potentials, and starting potential can be adjusted as needed. Proper selection of these values depends upon the redox potential of the analyte and the redox reaction rate. As the voltage is incrementally scanned between high and low values, the analyte will undergo redox reactions if the applied voltage corresponds to the minimum energy required to oxidize or reduce a redox-active species. Slower scan rates allow more time for a given reaction to occur at an applied voltage. Conversely, slow reversible redox reactions may not be observable if a voltage scan rate is selected such that insufficient time is allotted for the oxidation/reduction of the material of interest. Total peak current is related to scan rate via the Randles-Sevcik equation:

$$i_p = (2.69 \times 10^5)n^{3/2}AD^{1/2}C_iv^{1/2} \qquad (3)$$

Where i_p is peak current, n is the number of electrons transferred, A is the area of the electrode surface, D is the diffusion of analyte to the electrode surface, and v is the scan

rate. An experimental scan rate must therefore be low enough to allow the desired redox transformation to occur, but fast enough to yield an observable peak above the baseline of the scan.

An idealized CV scan for a fully reversible system is depicted in Figure 2.1. The output of a CV scan is a graph of current versus voltage. Voltage is changed at a constant rate, and thus each applied voltage generates a current to or from the sample. In this figure i_p^c is the cathodic peak current corresponding to the reduction of the analyte, while i_p^a is the anodic peak current corresponding to the oxidation of the analyte. Each peak is centered about a characteristic voltage for a given redox reaction called the anodic or cathodic potential. The anodic or cathodic potential is analagous to an activation energy and is a thermodynamic reaction constant for a given temperature and analyte speciation. For a fully reversible system the following simplified relationship is valid:

$$\Delta E = 0.058V/n \qquad\qquad (4)$$

Where ΔE is the difference in voltage between the anodic and cathodic potential and n is the stoichiometric number of electrons transferred. Using this relationship, a one-electron transfer in a reversible system should theoretically have a spacing of ~60 mV between the anodic and cathodic peaks. Systems that follow the relationship in Equation 2 are characerized as fully reversible. If ΔE is greater than 60mV/(mol of electrons transferred), the system is quasi-reversible. Several factors can cause a reversible redox system to exhibit quasi-reversible behavior in a CV experiment. Among the more common factors are competing chemical reactions that consume one or more members of the redox system and/or voltage scan rates that are too fast to allow full

15

oxidation/reduction. Fully reversible processes should have equal current ratios such that

$i^c/i^a = 1$, while quasi-reversible reactions will demonstrate deviations from unity.
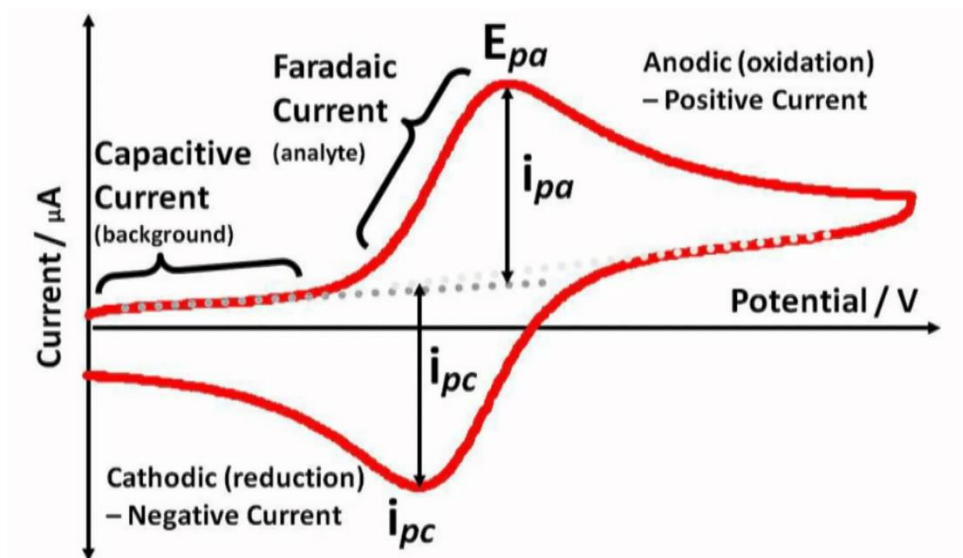

Figure 2.1. Theoretical CV scan of a reversible redox system. E_p^a is the anodic peak potential, and i_p^a is the current at this point. E_p^c is the cathodic peak potential, and i_p^c is the current at this point.[32]

Prior to the onset of an applied cyclical voltage, the sample can be held at a

constant voltage for a set period of time. This "preconditioning" allows a sample to be

conditioned to a desired initial oxidation state. For example, a negative preconditioning

of the sample allows one to remove any oxidation products on the surface of an electrode

that has been exposed to an oxidizing environment (*e.g.*, bench top storage). In this way,

the electrode surface at the start of each run is consistent. If the prospective redox system

is well characterized, proper selection of the preconditioning voltage, scan rate, and

voltage limits allow specific redox transformations to be induced and characterized.

Thus, CV is a useful technique to examine the effect of physical factors (such as pH, concentration, and temperature) on the redox-induced changes of a given analyte.

Summary

Redox reactions that lead to the mobilization of uranium are a very important potential cause for uranium release in a disposal scenario. Uranium incorporation into hematite presents interesting possibilities with regard to future immobilization of uranium leached from corroded spent nuclear fuel. However, *a priori* knowledge of the relevant electrochemical properties of uranium incorporated into hematite is limited. The body of research that has explored the environmental parameters of uranium sorption onto Fe-bearing minerals and compounds has not yet been extended to uranium incorporation into iron minerals[8,9,10,11,33]. Although uranium incorporation into proximal minerals is a growing area of research, published work has largely focused on characterization of the structure and composition of the incorporated mineral form[22,23]. Electrochemical properties of the incorporated uranium remain largely unknown. Consequently, it cannot be assumed that, in a given environment, uranium incorporated into hematite will undergo the same electrochemical reactions as sorbed uranium; rather, the differences in chemical environment are likely to translate into different electrochemical properties. Given the long time scales of interest for evaluating risk at a geologic repository, experimental methods that can rapidly probe and/or induce electrochemical changes are necessary to explore the possible electrochemical transformations of incorporated uranium.

CHAPTER THREE

Hypothesis and Objectives

The overarching hypothesis of this work is that uranium incorporated into hematite can undergo electrochemical changes that are dependent on the physical environment of the hematite sample. This hypothesis implies three subsidiary hypotheses:

(1) Uranium can be structurally incorporated into hematite via direct substitution for Fe(III) ions.

(2) Uranium incorporated into hematite undergoes electrochemical reactions that reversibly cycle between the (V) and (VI) oxidation states.

(3) The thermodynamic viability and kinetic favorability of uranium redox reactions are sensitive to the external parameters of pH, temperature, electrolyte composition, and host crystallinity.

The research objectives of the proposed work are dictated by these hypotheses and are similarly threefold:

(1) Verify that uranium can be directly incorporated into hematite.

(2) Identify the different redox behavior of U structurally incorporated in hematite *versus* U sorbed onto hematite powders.

(3) Evaluate the effect of changing environmental conditions, notably pH and temperature, on the kinetic and thermodynamic properties of the uranium redox reactions.

CHAPTER FOUR

Materials and Methods

Synthesis and Characterization

The U-doped hematite synthesis was adapted from previous methods[22,23]. An 850 ml solution with a concentration of 0.18 mM $UO_2(NO_3)$ (Electron Microscopy Sciences CAS #13520-83-7) was sparged with nitrogen for two hours. While continually sparging with nitrogen, 1.7 g of $FeCl_3$ (Amresco CAS #7782-61-8) and 5.1 g of $NaNO_3$ (Amresco CAS #7631-99-4) were then added to the solution. Sodium hydroxide was added drop wise to raise the pH to ~7, and the solution was then sparged with nitrogen and stirred for two hours. A final addition of sodium hydroxide was used to raise the final solution pH to ~11, and the solution was sparged with nitrogen and stirred for one and a half hours. For fully crystalline samples the solution was then incubated for 28 days at 90 degrees Celsius. These U-doped hematite samples were used in all CV experiments, except for those examining the effects of aging on uranium incorporation, where U-doped hematite samples were incubated for 3, 7, 14, and 28 days. Undoped hematite samples were prepare using the same methodology, including the 28 day incubation period for better comparison with the U-doped hematite samples.
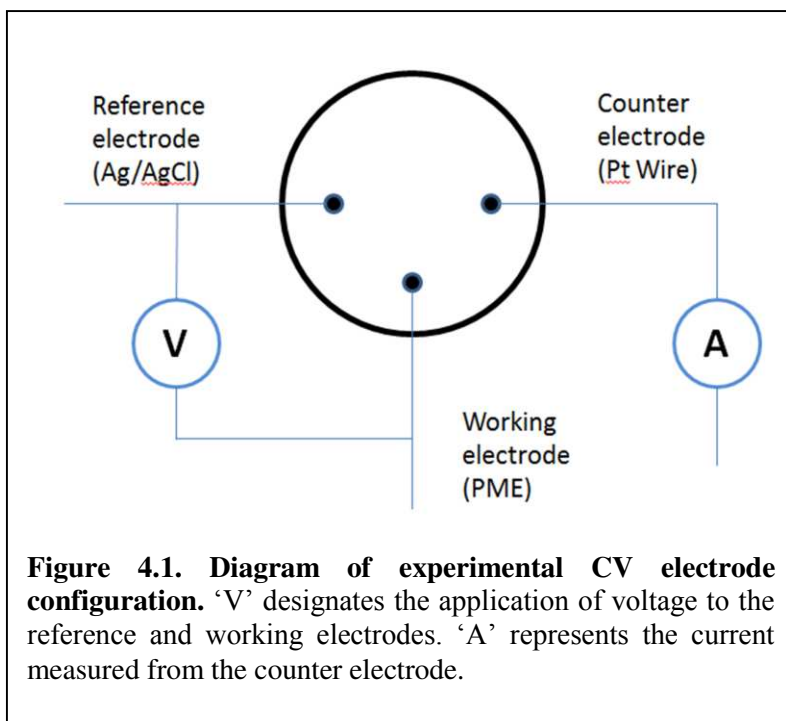
After incubation, 650 ml of the solution was decanted while taking special care to avoid removal of the settled solids. The remaining solution was transferred to a 250 ml centrifuge bottle, shaken by hand, and centrifuged at 9000 rpm for ten minutes. The solution was decanted and rewashed five times with 150 ml of 0.5 M $CaCO_3$. This

process was then repeated for at least five wash cycles using DI water. The residual solids were dried for two hours at 70 °C. The supernatant was diluted to a 10:1 ratio with 2% nitric acid to a total volume of 10 ml, and analyzed for uranium and iron concentration using a Thermo Scientific X Series 2 inductively coupled plasma mass spectrometer (ICP-MS).

The solid phase was characterized using X-ray diffraction (XRD), scanning electron microscopy (SEM), and transmission electron microscopy (TEM). All XRD measurements were completed on a Rigaku Ultima IV powder diffractometer. Measurements were collected between 2Θ values of 15-65° at a scan rate of 0.5° per minute. SEM images were collected on a Hitachi FESEM 4800 using an accelerating voltage of 15 kV with an emission current of 15 μA. Energy Dispersive X-Ray Spectroscopy (EDS) was collected on an Oxford INCA system with a SiLi detector. TEM images were collected on a Hitachi TEM 7600.

Experimental Set-up

Cyclic voltammetry (CV) commonly uses three electrodes (Figure 4.1) immersed in an electrolyte solution. Voltage is applied to the sample at the working electrode as desired. A second

Figure 4.1. Diagram of experimental CV electrode configuration. 'V' designates the application of voltage to the reference and working electrodes. 'A' represents the current measured from the counter electrode.

electrode of known voltage serves as the reference electrode, with a third electrode serving as the counter electrode. In all experiments presented here, an Ag/AgCl reference electrode was used, along with a Pt wire counter electrode. Measurement sensitivity was enhanced by the use of a cavity microelectrode (CME), referred to in this thesis as a powder microelectrode (PME). A PME is advantageous when studying systems that require fast voltage scan rates to observe redox reactions of interest. As scan rate increases, conventional electrodes generate an unacceptable level of charging current that severely deteriorate analytical resolution; however, the high surface area of a PME helps to negate this effect[34,35]. In PME, the analyte (*i.e.,* U-doped hematite) serves as the working electrode and is packed into a small micro-cavity with a diameter of either 50 or 100 μm, depending on the size of the Pt wire. In conventional CV, bulk diffusion is required to bring an aqueous analyte into contact with the working electrode. Since the lateral surface area in the cavity of a PME is quite small, diffusion effects related to the movement of cations crossing the electrode surface are minimal. If the micro-cavity is packed with a consistent volume of uniformly sized analyte particles, total current does not vary since the concentration of analyte at the electrode surface is constant. Measurement reproducibility is ensured with the comparison of the open circuit potential (OCP) at the onset of each experiment.

For all CV experiments the background electrolyte was a 0.05 M sodium sulfate solution. Prior to application of pre-conditioning voltage, the test cell was sparged with argon for thirty minutes. The voltage was held at an initial potential of -0.35 V for 50 minutes, and then cycled between 0.7 and -0.7 V at a scan rate of 50 mV/s. The pH of the

21

electrolyte solution was adjusted using NaOH and HNO_3. Then pH ranged from 2.5 to 12.5. A second series of experiments examined the effect of changing temperature. Temperature was lowered by submerging the glass reaction cell into an ice bath. Similarly, temperature was elevated by submerging the reaction cell into a water bath on a hot plate. A thermometer with dual thermocouple leads was used, with the leads inserted directly into both the ice/water bath and the electrolyte solution to insure equilibration to the desired reaction temperature. In all experiments, aliquots of the electrolyte solution were retained for ICP-MS analysis of uranium and iron. ICP-MS measurements of the electrolyte solution were conducted in the same manner as previously indicated for the washing supernatant. A PAR 273A potentiostat was used for the variable pH experiments, and a Versastat 3 potentiostat was used for the temperature and aging experiments. Princeton Applied Research (PAR) software was used for data collection and initial analysis.

Data Analysis

Quantitative analysis of CV data was completed using Origin Pro 9 software. The method used to determine CV peak area is illustrated in Figure 4.2. A line was superimposed along the baseline of the CV data spectrum beginning at 0 V. The voltage at which current deviated from this line was defined as V_1 and signifies the onset of the peak. A local minimum was observed between the U(IV) and Fe(II) oxidation peaks. The voltage corresponding to this minimum current, V_3, was defined as the maximum value of the peak. Voltage V_2 was defined, prior to the maximum anodic current, as the

voltage which corresponded to the same value of current observed at V_3. Area 'a' as shown in Figure 4.2 was then integrated between V_2 and V_3. Area 'b' was integrated between V_1 and V_3. The total area of the peak was defined as area 'a' plus one half of area 'b.'
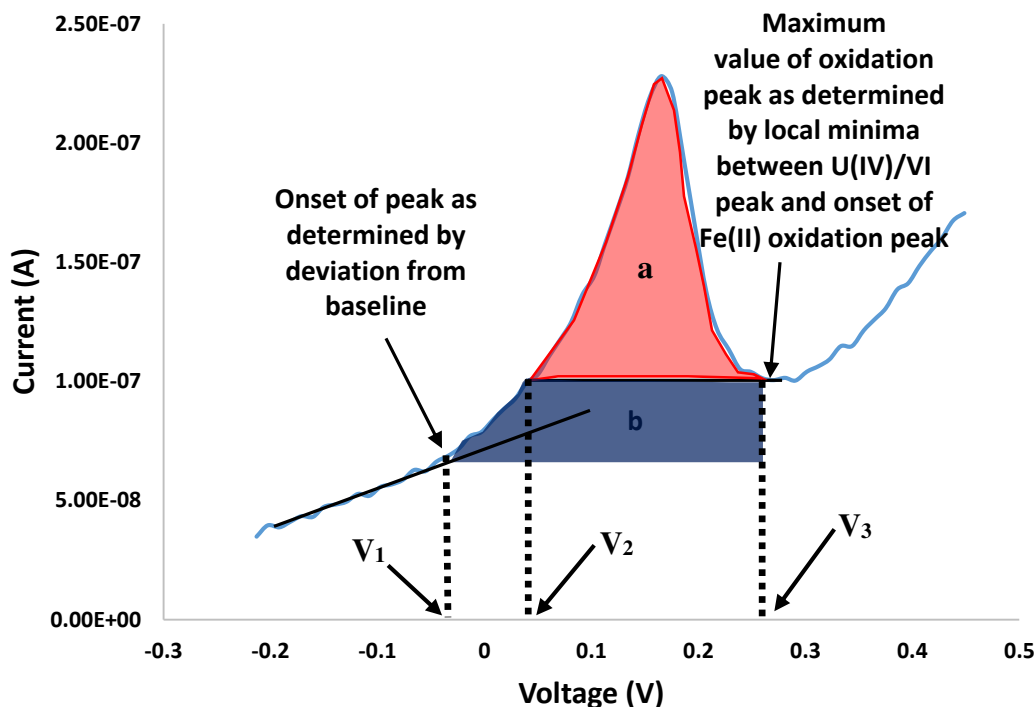

Figure 4.2. Demonstration of method used to quantify peak area. Voltage V_3 is defined at the maximum of the anodic peak. Voltage V_1 is defined at the onset of the anodic peak. Voltage V_2 is defined, prior to the maximum current value of the anodic peak, at the same same current as V_3. The total anodic peak area was defined as the sum of area 'a' plus one half of area 'b.'

The peak potential was defined as the potential that corresponded to the maximum value of current at a defined redox peak. The method used to define the full width half maximum (FWHM) is illustrated in Figure 4.3. Voltage V_1 is defined the same way as previously described. Voltage V_2 is defined as the voltage that occurs at the maximum current of the U(IV) oxidation peak. V_3 is then determined as $(V_1 + V_2)/2$. V_4 occurs at

the current, prior to V_2, that also occurs at V_3. The FWHM is the voltage difference
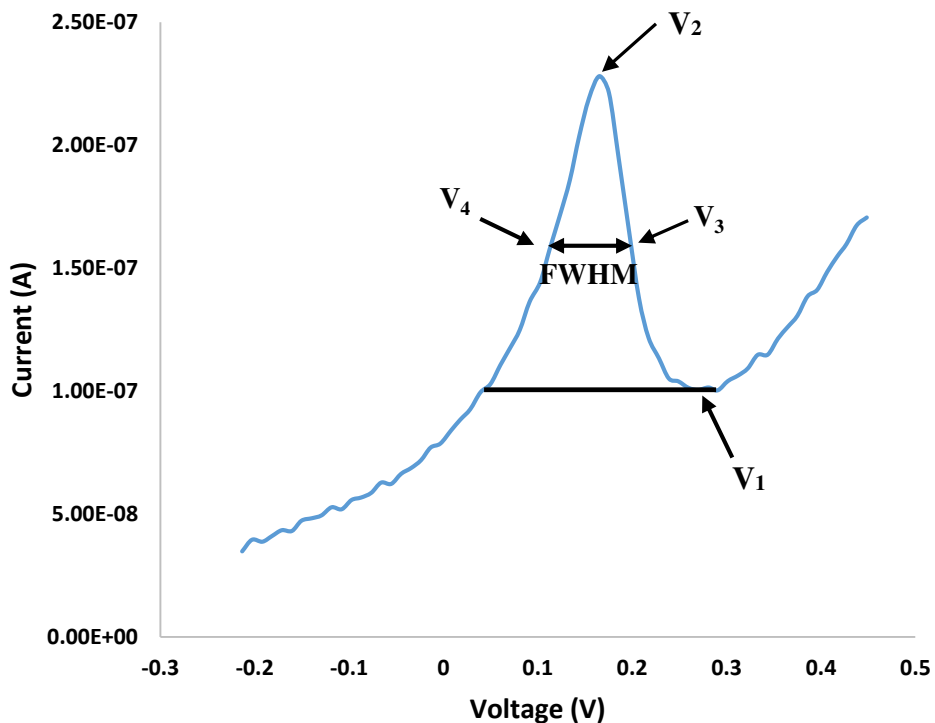
between V_3 and V_4.

Figure 4.3. Determination of FWHM. Voltage V_1 is defined at the maximum of the anodic peak. Voltage V_1 is defined at the onset of the anodic peak. Voltage V_2 is defined at the maximum current of the anodic peak. V_3 is defined as $(V_1 + V_2)/2$. V_4 occurs at the current, prior to V_2, that also occurs at V_3.

CHAPTER FIVE

Results and Discussion

Analysis of Uranium Doped Hematite

Supernatant collected from each cycle of the sample washing sequence was analyzed for uranium and iron content using ICP-MS (Figure 5.1). Measurements were taken in triplicate, with the standard deviation used to calculate error. Corollary data from eight successive carbonate wash cycles is given in Figure A.2. The higher concentration of uranium in initial wash cycles (490 ppb) is due to the presence of uranium reversibly sorbed on the hematite surface. The amount of uranium removed by the carbonate wash reaches an equilibrium at about 100 ppb. Further carbonate washes do not remove more uranium (Figure A.2). As expected, the DI washes removed little remaining uranium (~ 5 ppb). The mass of uranium removed during ICP washes (~0.3 mg) is approximately 1% of the total mass of uranium initially used during synthesis of the doped hematite (0.0821 g $UO_3(NO_3)(H_2O)_9$). The mass percent of uranium in the sample was determined by digestion of a known mass of doped hematite (0.0122 g). Since the volume of the digested sample was known, the total uranium mass in the hematite sample was determined by ICP-MS to be 2.016 µg. Thus, the doped hematite sample was 16 wt% uranium, which corresponds to a 6.7% U:Fe atomic ratio. All CV experiments, except those that examined the effect of aging, used this U-doped hematite sample in the PME. The 1% of uranium not irreversibly associated with the hematite sample either remained in the original synthesis supernatant or was reversibly sorbed to the hematite surface and

removed during the wash cycles. Due to edge and kink sites on the mineral surface, it is probable that some uranium remained sorbed to the surface after the completion of wash cycles.
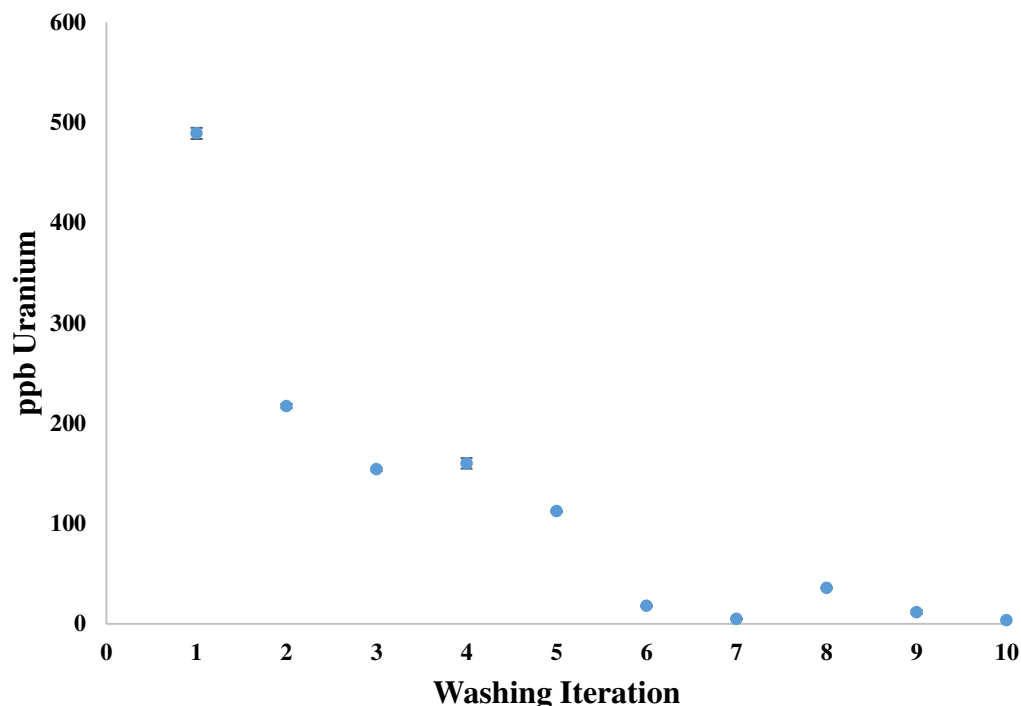

Figure 5.1. ICP analysis of uranium in supernatant following successive wash cycles of U-doped hematite. The first five iterations were conducted with 0.5 M calcium carbonate, and the final five used DI water. Error bars represent the standard deviation associated with each measurement.

SEM with energy dispersive spectroscopy (EDS) was used to confirm the presence of uranium associated with the hematite particles. EDS only indicates the uranium within approximately ten microns of the sample surface, and does not differentiate between sorbed or incorporated uranium. Figure 5.2 shows a representative SEM image of the U-doped hematite particle, with the inset showing the EDS spectrum

associated with the indicated area. This data is representative of each synthesized sample

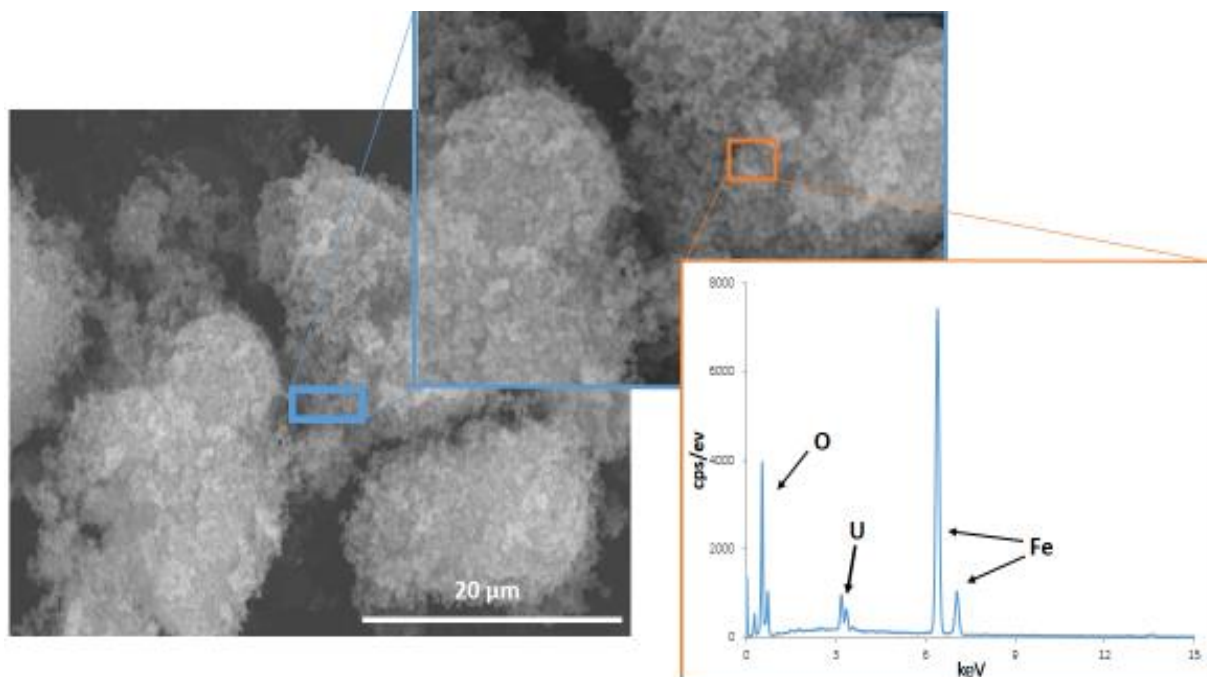and indicates the association of uranium with the hematite particles.

Figure 5.2. SEM image and EDS spectrum of U-doped hematite sample with selected location for EDS analysis annotated on mineral surface. Iron, U and O are clearly present in the sample. Additional SEM images are given in Figure A.3 – A.4

Figure 5.3 shows the high XRD spectral correlation observed between U-doped hematite

and undoped hematite, which was synthesized using the same method as previously

described. The sharp peaks and low background of the XRD spectra indicate a high level

of crystallinity. Overlap between the undoped and doped spectra corresponds to hematite

peaks. The undoped sample contained small amounts of goethite (Peak I in Figure 5.3) A

relative intensity ratio analysis was performed, where theoretical intensities of the

strongest hematite and goethite peaks are obtained from reference data in the powder

diffraction file (pdf) of the mineral. Peak intensity data in the pdf is relative to an

aluminum standard. Using theoretical intensities, the intensity ratio of a theoretical 50:50

hematite:goethite mixture is calculated. The actual intensity ratio is then proportional to

the composition of the sample. Using relative intensity ratio analysis, the undoped

sample was estimated to include 18 ± 5 weight % goethite. Goethite formation does not

appear to be a systemic by-product of the synthesis method since multiple doped samples

were synthesized without measureable goethite. Slightly higher incubation temperatures,

additional moisture content at the onset of the drying process, or elevated drying

temperatures are all variations that may have contributed to the formation of a goethite

phase. All samples were stored at room temperature after drying for several months

during analysis. However, the absence of goethite from doped samples does not indicate

that goethite systematically formed during the storage phase.

The doped samples also contain several peaks in addition to hematite that may be

indicative of an additional mineral phase. Peaks II and III in Figure 5.3 illustrate the

highest intensity peaks attributed to the uranium mineral clarkeite, which has the generic

formula $(Na)(UO_2)O(OH) \cdot H_2O$[36]. From relative intensity ratio analysis, clarkeite was

measured as 14.5 ± 7 weight % (0.8 atomic %) in the hematite sample. Clarkeite is

relatively rare in nature, but is found intermingled as a co-precipitated phase with other

uranium minerals. As the mineral is a high-temperature hydrothermal by-product, its

formation is consistent with the methods employed for hematite synthesis. Additional

crystallographic analysis is necessary to provide further evidence of this mineral phase

and to better characterize its distribution. At this point it remains unclear whether

clarkeite forms a separate precipitate intermixed with the hematite particles, or whether

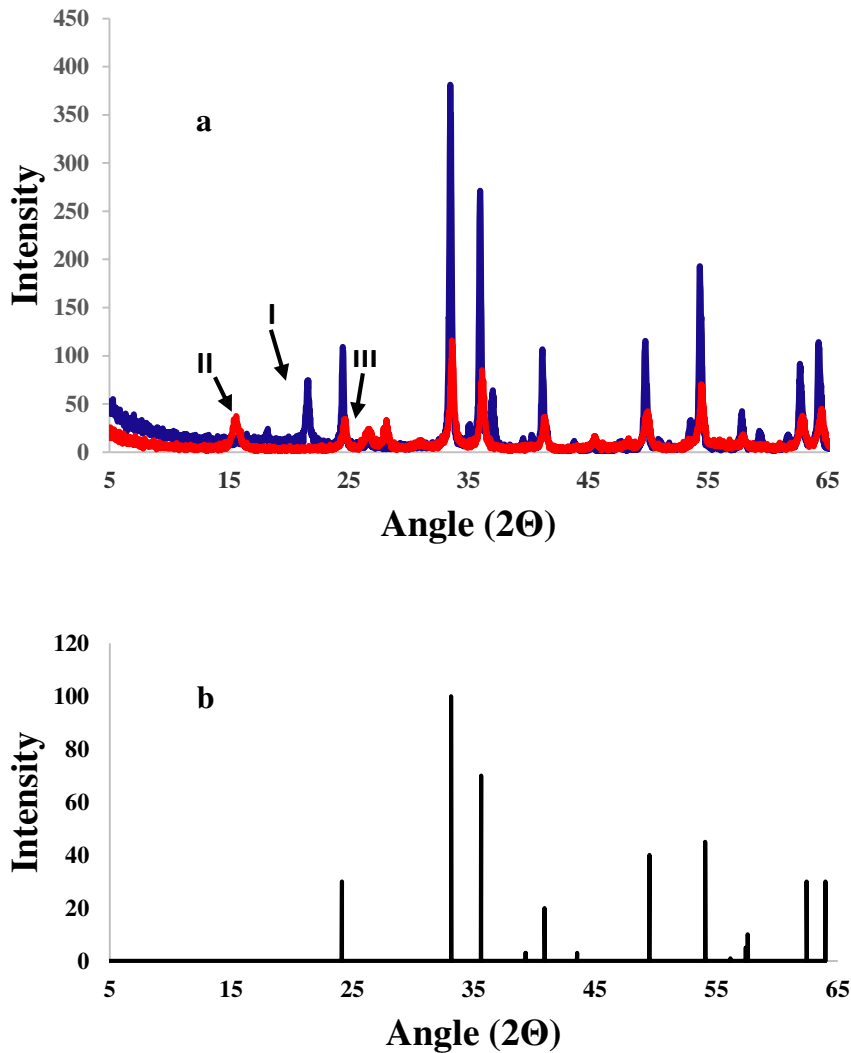clarkeite is primarily found as a co-precipitated surface phase.

Figure 5.3. a). XRD spectrum of uranium-doped hematite incubated for 28 days. Peaks I and II correspond to a uranium alteration phase (identified as clarkeite) in the doped sample. b) **Reference XRD spectrum of synthetic hematite.**

The spectrum of the doped sample also indicates a slight peak shift to higher 2θ

angles relative to both the undoped hematite and hematite reference standards. This shift

indicates a decrease in the lattice parameters of the hematite structure. The ionic radius

of U(VI) is slightly larger than Fe(III). However, substitution of the uranium into hematite requires an iron vacancy. Figure 5.4 depicts a model of hematite in which U(VI) is octahedrally coordinated in a vacated Fe(III) layer. The exact substitution mechanism remains unclear, but this substitution mechanism shows the possibility for the unit cell to compress with U(VI) substitution, which causes the observed peak shift.
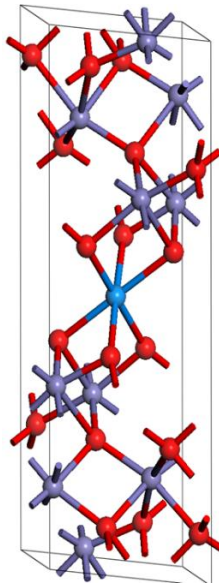

Figure 5.4. Molecular model of uranium-doped hematite structure. The center blue atom is U(VI), red atoms are oxygen, and purple atoms are Fe(III).

Figure 5.5 is a high resolution (HR) TEM spectra of hematite, which clearly depicts the crystalline structure of the sample. Lattice fringes (and even atoms) are clearly observed in the HR-TEM micrograph, which is indicative of a highly crystalline sample. Darker areas are most likely caused by localized increases in sample thickness due to overlay of mineral particles. Although uranium was detected by EDS of the sample and clarkeite was identified by XRD, there was no visual confirmation of an additional mineral phase. This may be due to a low percentage of clarkeite in the sample,

compounded by the small sample size necessary for TEM work. D-spacing values of the mineral were measured twice with the TEM, with obtained values of 1.756 Å and 2.234 Å. These values are greater than 0.2 Å away from the closest pdf d-spacing values for hematite or clarkeite. This discrepancy may be due in part to TEM calibration, but may also be due to previously described changes in the lattice parameters caused by uranium incorporation. The sample appeared to be morphologically homogeneous. (Figure A.5) The absence of an observable uranium alteration phase, and the shift in the diffraction peaks relative to theoretical values, may thus be consistent with structural alteration caused by uranium incorporation. This possibility is strengthened by the fact that both clarkeite and hematite belong to the R3 space group and therefore have the same symmetry, which increases the likelihood that the diffraction patterns will be similar.
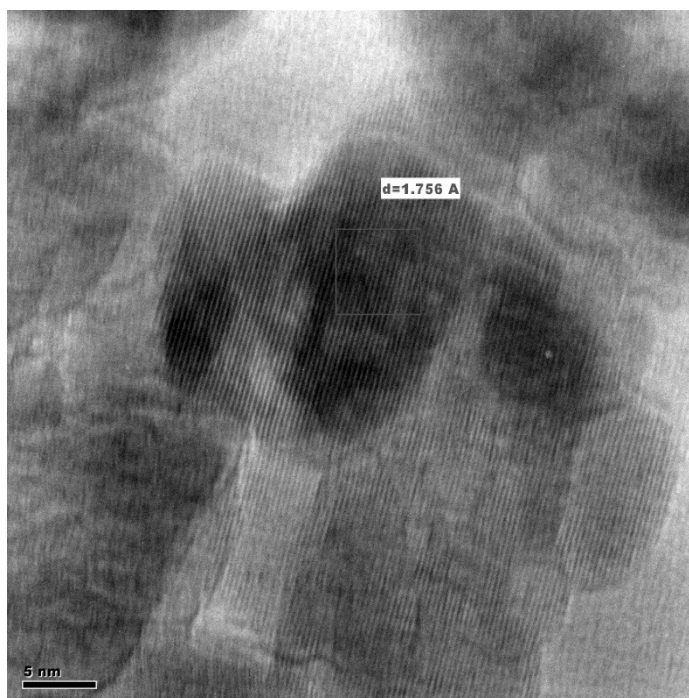
Figure 5.5. TEM image of uranium doped hematite sample. The lattice fringes show the crystallinity of the hematite particles with a measured d-spacing of 1.756 Å.

CV Analysis of U-doped Hematite

The CV data for U-doped hematite is given in Figure 5.6. The oxidation potential for the U(IV/VI) oxidation(~ 0.15V) and U(VI/V) reduction (~ 0.20 V) of uranium sorbed onto hematite is known from a prior literature study[29]. In Figure 5.6, the peak at about 0.2 V (Peak I) corresponds to a U(IV) oxidation to U(VI), accompanied by a reduction at about -0.2 V from U(VI) to U(V) (Peak II). A smaller peak at about 0.0 V in cycle 2 (Peak II) corresponds to the oxidation of U(V) to U(VI); the separation between the peaks (~ 0.5 V) indicates a quasi-reversible redox couple between U(V) and U(VI). To confirm that these peaks were attributable to uranium redox, a control CV experiment of undoped hematite was completed (See Figure A.6).
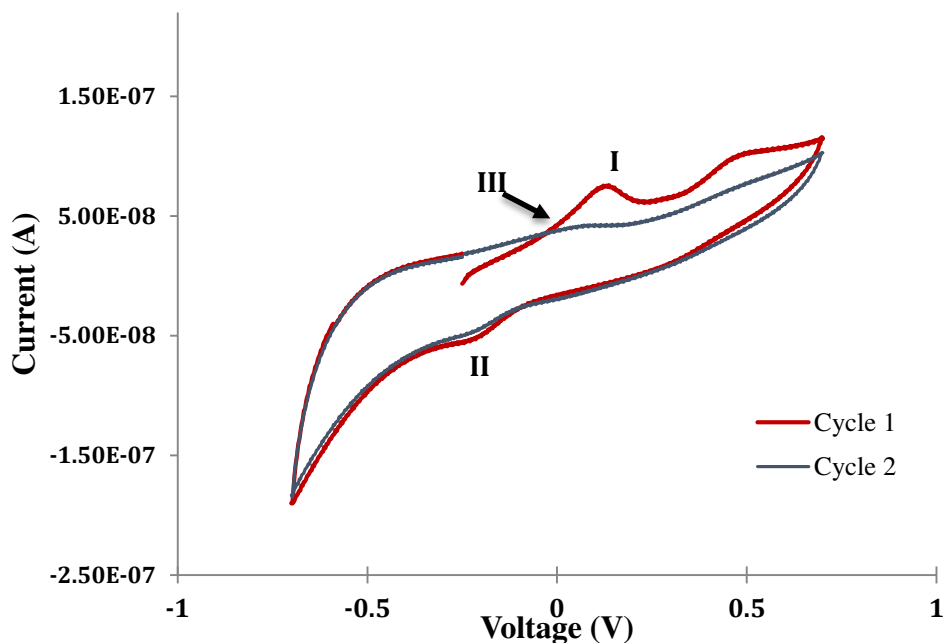
Figure 5.6 CV scan of U-doped hematite. Peak I corresponds to the irreversible U(IV) to U(VI) oxidation following preconditioning. Peak II corresponds to the reversible U(VI) to U(V) reduction. Peak III corresponds to the U(V) to U(VI) oxidation. The sample was preconditioned at -0.35V for 50 minutes in a 0.05 M sodium sulfate electrolyte solution at pH 3.5. The voltage scan rate was 50 mV/s.

The U(V)/(VI) couple persists in subsequent scans, unlike the U(IV)/(VI) couple.

The voltage separation of approximately 0.5 V between peaks indicates that the U(VI)-

U(V) couple is quasi-reversible. The most probable cause for quasi-reversibility is that

the kinetics of either the oxidation or the reduction reaction is slower than the scan rate.

Given the smaller area of the U(V) oxidation peak relative to the U(VI) reduction peak, it

appears most likely that the cycling limits U(V) oxidation.

Typically, U(V) disproportionates to U(IV) and U(VI), although some

stabilization is possible when incorporated into solid phases[23].   In the case of aqueous

uranyl species, disproportionation typically occurs as follows:

$$2UO_2^+ \longrightarrow UO_2^{2+} + UO_2(s)$$
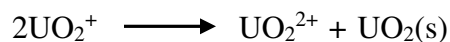
The free energy of UO_2 is lower than UO_2^{2+} and tends to drive the disproportionation process. It should be noted that specific thermodynamic data for incorporated uranium is not yet available, and thus it is not known with certainty whether the stability of U(IV) also drives the disproportionation of incorporated U(V). The absence of U(IV) oxidation after the first cycle in Figure 5.6 indicates that the rate of disproportionation is slower than the voltage scan rate used during experiments. Thus, insufficient time is given for disproportionation, and U(V) is directly oxidized to U(VI) upon application of a sufficient positive voltage on the forward scan.

The initial concentration of U(IV) is present from the reduction of U(VI) due to preconditioning of the cell at -0.35 V for 50 minutes. The magnitude of the anodic peak can be increased by either lowering the preconditioning voltage or extending the preconditioning time. Figure 5.7 demonstrates the effect of preconditioning time for sorbed uranium. The increase in current at the anodic peak indicates a higher proportion of uranium initially converted to U(IV) that was subsequently available for oxidation back to U(VI). Longer pre-conditioning times allow the ingrowth of more U(IV) from the reduction of U(VI) and disproportionation of U(V).
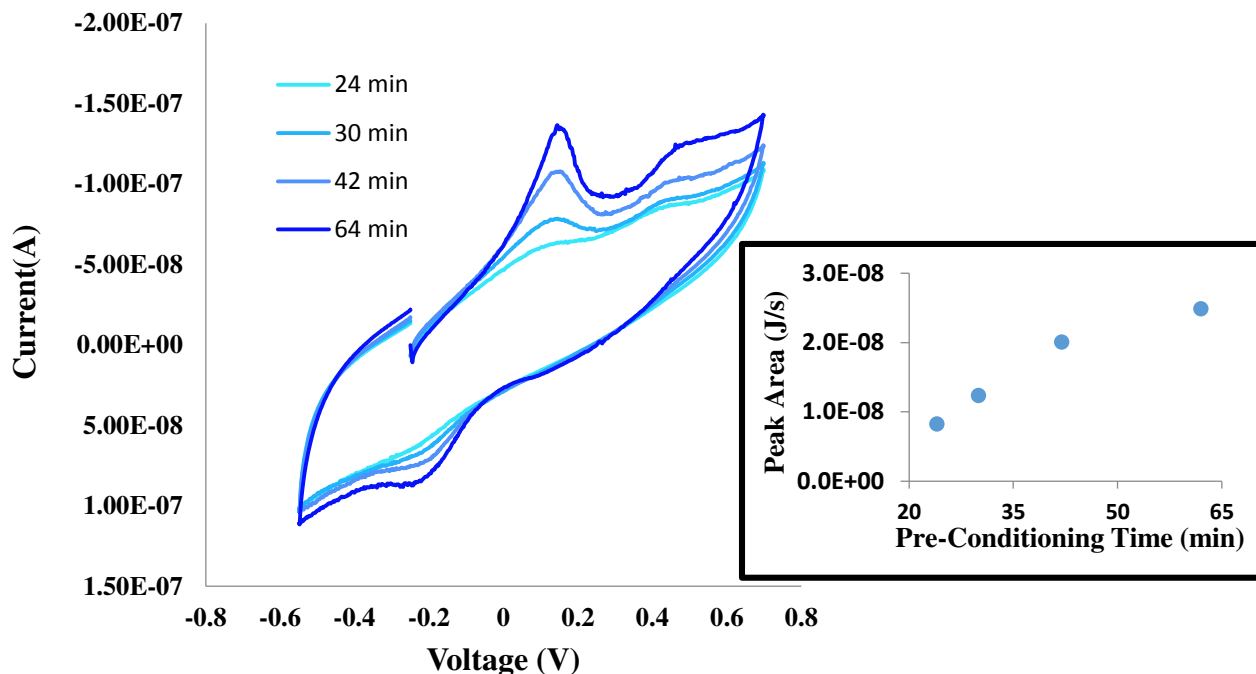
Figure 5.7. Redox of sorbed uranium on a hematite PME as a function of preconditioning time. Only the first scan cycle is depicted, which results in an apparent discontinuity at -0.35V. The preconditioning voltage was -0.2 V and the preconditioning times included 24, 30, 42, and 64 minutes. The inset shows the quantification of the anodic peak area *versus* pre-conditioning time.

Total peak area is a direct function of the total mass of material undergoing the oxidation change. Therefore, Figure 5.7 depicts increasing quantities of U(IV) being oxidized to U(VI), which indicates greater initial reduction of U(VI) with increasing preconditioning time. Extended preconditioning times and/or lower preconditioning potentials also increase the concentration of Fe(II). The subsequent oxidation of Fe(II) to Fe(III) is seen at about 0.5 V in Figure 5.7. Because hematite is an Fe(III) oxide, iron reduction may alter the structure and allow for the release of incorporated uranium. For electrolyte solutions with pH greater than 4.0, ICP-MS results show that the U and Fe concentrations in the background electrolyte are below the detection limit (4.0 ppb Fe and 0.002 ppb U).

Figure 5.8 illustrates the equilibrium attained for the uranium-doped hematite system over multiple cycles. The time required for the U(VI) to U(IV) reduction is longer

than the voltage scan rate; therefore, this redox couple is effectively irreversible for these experimental conditions. Note that irreversibility does not denote that the re-reduction of U(VI) to U(IV) is thermodynamically unfavorable. Rather, the kinetic time scale is slow relative to the voltage scan rate.
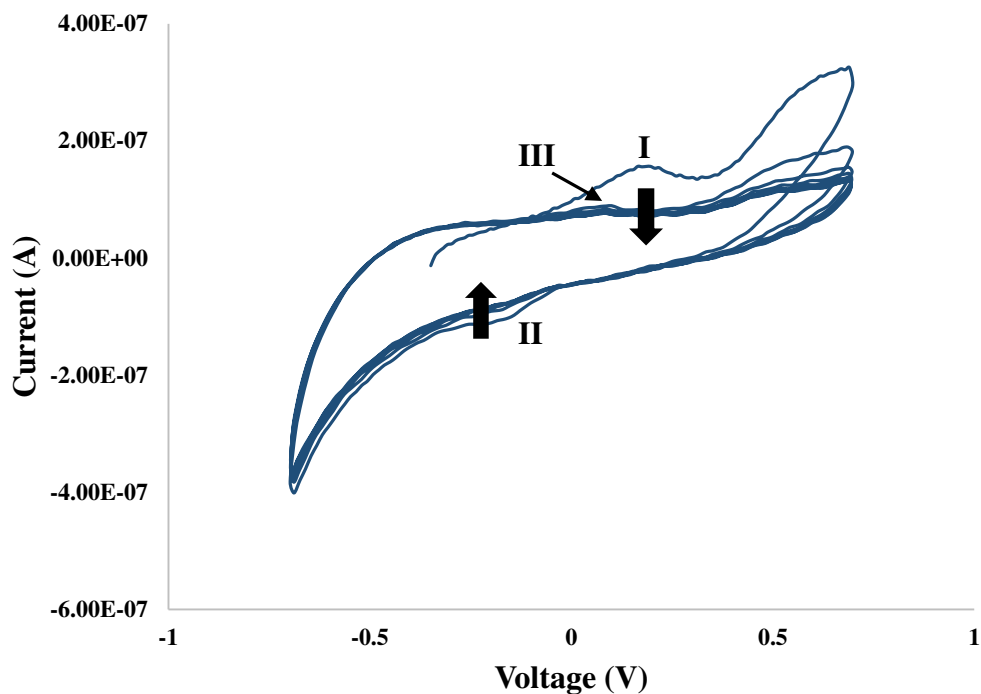

Figure 5.8. CV scan of uranium-doped hematite for eight cycles. Peaks I, II, and III are analogous to those described in Figure 5.1. Peak I appears only in cycle 1, whereas peaks II and III appear in each cycle and approach an equilibrium value. Arrows point in direction of increasing cycle number.

As seen in Figure 5.8, the intensity of the U(VI) to U(V) peak decreases and approaches a steady state after approximately seven cycles. During the first cycle the large population of U(IV) generated during preconditioning is oxidized to U(VI), which is in turn reduced to U(V). A smaller amount of U(VI) is generated in subsequent cycles from the oxidation of U(V). Therefore, the mass of uranium oxidized to U(VI) is much

lower after cycle one, which causes the total peak current in the U(VI)-U(V) couple to decrease as well. The total peak area decreases as equilibrium is reached. The peak area of the U(V) to U(VI) oxidation peak decreases by 23% between cycles 2 and 3, 18% between cycles 3 and 4, and ~ 1% or less between all subsequent cycles.

The same behavior of U(IV) to U(VI) oxidation in cycle one, followed by only U(V) to U(VI) oxidation in subsequent cycles, is also observed for uranyl sorption onto hematite (Figure 5.9). The anodic peak areas (1.12 E-08 J/s for incorporated uranium versus 1.35 E-08 J/s for sorbed uranium) indicate that comparable amounts of U(IV) are oxidized in both systems. However, the U(IV)/(VI) anodic peak potential is shifted to ~ 0.25 V, as compared with the anodic peak potential of ~0.15 V for U-doped hematite. This shift is consistent with an alteration to the U(IV) oxidation potential due to the different chemical environment of incorporated uranium
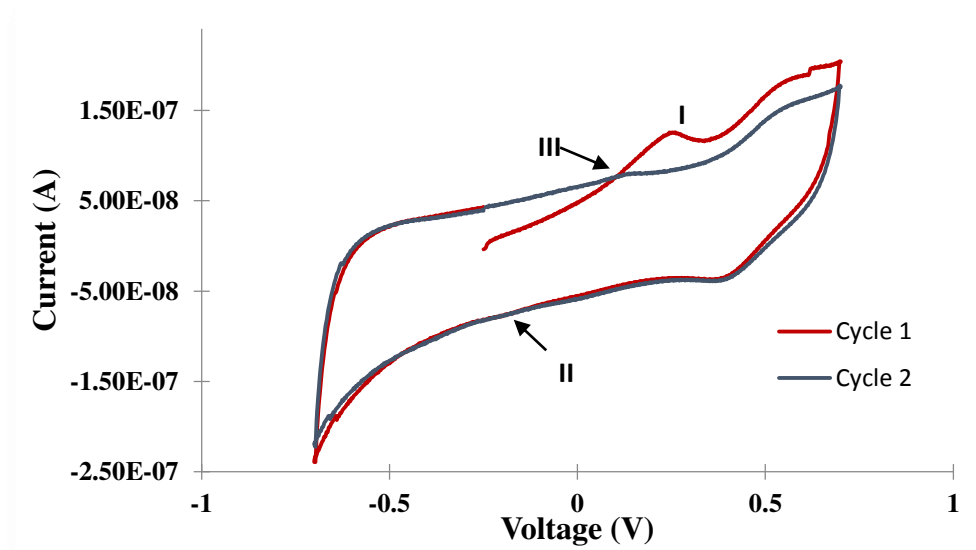

Figure 5.9 CV scan of undoped hematite with 0.5 mM of uranyl nitrate in a 0.5 M NaSO₄ solution at pH 3.5. Peak I corresponds to the irreversible U(IV) to U(VI) oxidation following preconditioning. Peak II corresponds to the U(VI) to U(V) reduction. Peak III corresponds to the U(V) to U(VI) oxidation. Peaks II and III form a quasi-reversible couple.

Ilton et al (2012) studied the reduction of uranium in a doped hematite system and found that U(V) was the dominant species upon reduction of U(VI). It was proposed that U(V) is more stable in an octahedral coordination environment than U(VI), which naturally favors reduction to U(V) for incorporated uranium. Ilton found that U(VI) reduction to U(IV) was preferred for non-incorporated uranium on the surface of the mineral. U(IV) in our experiments may thus be indicative of a significant population of uranium on the surface.   However, a fundamental difference occurs in that an external source of electrons is available in the CV studies to force the oxidation state of uranium to U(IV). Due to the application of external energy, the thermodynamic limitations that restrict the formation of U(IV) in Ilton's work may not be evident in our system. Ilton also reported that, at pH 7.1-7.3, incorporated U(V) was stabilized between an eH range of -0.21V to 0.25V. Our CV experiments are consistent with these findings in that U(VI) is reduced to U(V) at approximately -0.20V and is oxidized to U(VI) at approximately 0 V.

Characterization of Uranium Redox at Varying pH Conditions

The structure of hematite becomes unstable below pH ~ 3, at which point the mineral begins to dissolve[37]. Matrix dissolution will lead to the release of incorporated uranium into solution. Upon release from the crystalline matrix, the U(VI) ions will likely form uranyl ions in solution; however, the actual speciation of released U(VI) depends on the ambient chemical environment, pH, and eH values[38]. For example, hydroxylated uranyl complexes form at high pH, while acidic conditions favor the

speciation of uncomplexed uranyl molecules [27]. The total concentration of sorbed

uranium is also highly pH-dependent and decreases at low pH due to the positive surface

charge caused by the excess of H^+ at the mineral surface (See Figure A.1). Note that the

point of zero charge of hematite occurs at pH ~8.4, which corresponds to a positive

charge on the mineral surface below this pH value. These mechanisms have the collective

effect of changing the concentration of sorbed and/or incorporated uranium. Uranium

redox properties in doped hematite will likely change as a result.

To evaluate the effect of pH, CV experiments were run with a range of

environmentally relevant pH (between 2.5-12.5). Aliquots of the electrolyte solution

were retained for ICP analysis to identify any release of U or dissolution of the hematite

(Figure 5.10).

The concentration of iron is independent of pH above pH 3.5, indicating no

dissolution of the mineral into the electrolyte (Figure 5.10a). Elevated iron concentration

at pH 2.5 is consistent with hematite dissolution below pH 3.0. Visual Minteq[41] modeling

predicts that, at equilibrium and pH 2.5, 27% of iron by mass in hematite dissociates to

aqueous Fe(III). The exact mass of doped hematite powder used to pack the PME is

estimated to be about 1.1 mg. During CV experiments this mass of hematite is then

immersed in a sodium sulfate electrolyte solution. Any dissolved iron or uranium will

thus diffuse into the solution. The ICP-MS solution used in Figure 5.10 is a hundred-fold

dilution relative to the initial CV electrolyte solution. Thus, approximately 900 ng of iron

were dissolved from the hematite structure. This corresponds to 0.012% dissolution of

iron, which in turn indicates minimal bulk dissolution during the time scale of the experiment.

Any structural alteration of the hematite PME is expected to cause a release of incorporated uranium. Figure 5.10b demonstrates elevated uranium levels below pH 4. Since the sample is composed of 16 weight % uranium (6.7 atomic %), the percentage of total uranium leached into the electrolyte solution at pH 3.0 is 1.4%. Since iron release is not elevated above pH 3, the release of uranium between pH 3 and 4 may be release of sorbed uranium and/or surface uranium co-precipitates (*i.e.*, clarkeite). The stability of hematite decreases with pH, particularly at negative Eh values. Since the sample was pre-conditioned at a negative voltage, the possibility of structural alteration due to the formation of Fe(II) cannot be discounted. Structural alteration may in turn lead to a release of incorporated uranium. The concentration of uranium in solution is much higher relative to iron at all pH values. Experimental protocols require that the hematite be packed into a small cavity in the PME. At low pH, partial dissolution along grain boundaries may expose sorbed uranium in the interior of the packed mineral and facilitate release into solution. If this partial dissolution dislodges hematite grains from the packed micro-cavity, aqueous iron concentrations may not increase. It should be noted that, like iron, the mass of uranium released was approximately four orders of magnitude less than the total mass. While it is difficult to fully parse the contribution of sorbed *versus* incorporated uranium release at low pH, the total amount of uranium released is negligible compared to the total amount incorporated.
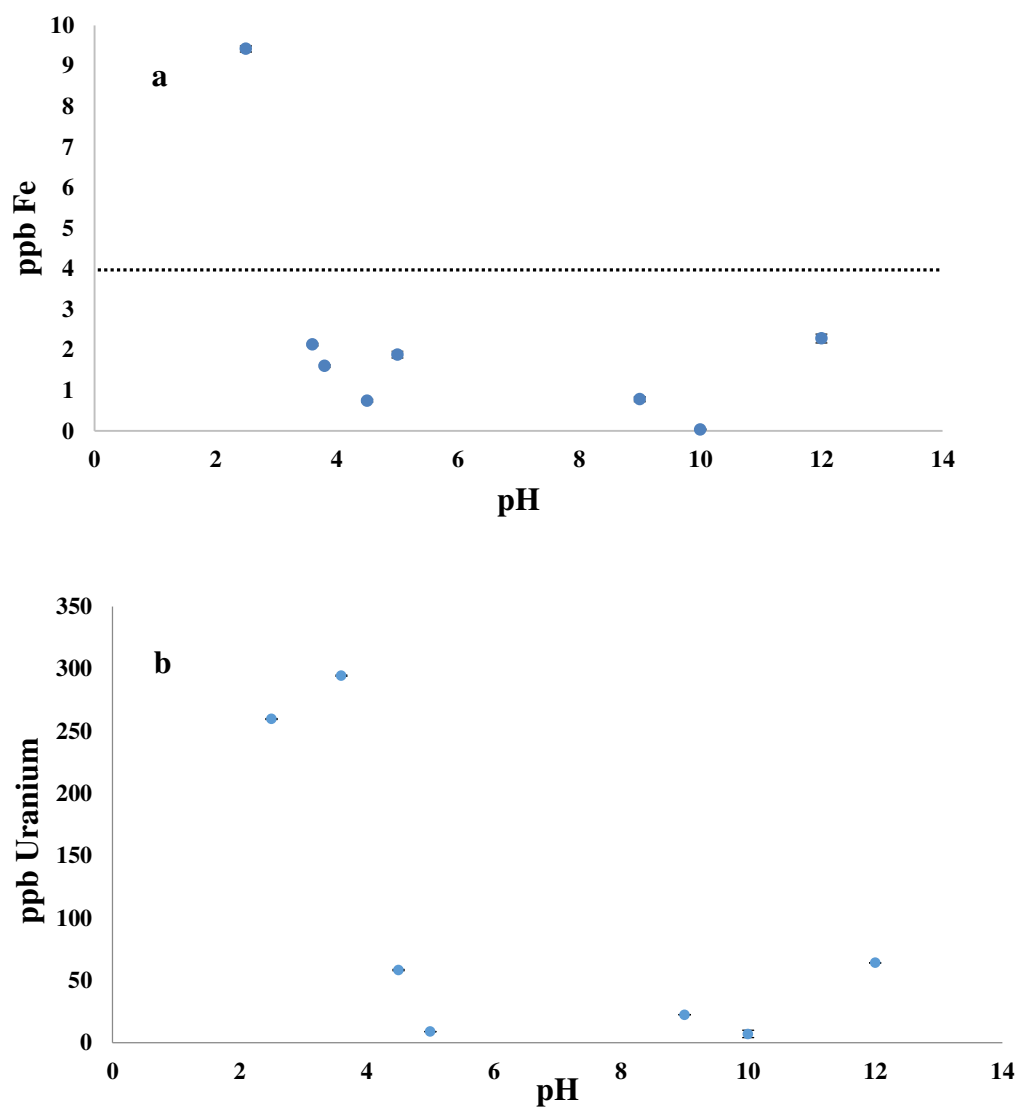
Figure 5.10. ICP-MS analysis of electrolyte solution following CV experiments at pH 2.5 to 12 showing concentration of Fe (a) and U (b). The dashed line in Figure 5.10a corresponds to the detection limit of the instrument. Error bars correspond to the standard deviation of the measurements.

CV scans were collected for doped hematite samples across the pH range 2.5-12.5, with select data shown in Figure A.7. At a pH of < 3.5, high current at both the U(IV) to U(VI) oxidation peak and U(VI) to U(V) reduction peak is observed. As with

Figure 5.1, the U(IV) oxidation peak disappears in subsequent scans, leaving the reversible U(V) - U(VI) couple. High peak current at pH < 3.5 is likely due to partial dissolution and/or alteration of the hematite structure, which then liberates uranium. Alternatively, pH may play an as-yet undetermined mechanistic role in the uranium redox reaction. In the CV experimental data shown in Figure A.7, reduction of incorporated U^{6+} is expected to occur as follows.

$$U^{6+} + 2e^- \longrightarrow U^{4+}$$
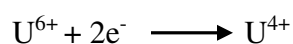
In this case, electrons are externally supplied by the potentiostat. Non-incorporated uranium speciation varies with pH due to the formation of uranyl sulfate and uranyl hydroxide species, as shown in Table 5.1. Although ICP-MS data from the sample washing indicates that approximately 1.4% of total uranium is sorbed, the contribution of sorbed versus incorporated uranium to total current is not yet known with certainty. pH induced changes to surface uranium speciation may thus play a significant role in changing peak potential and total current. At pH ~ 2.5, identifiable uranium redox peaks disappear. (Figure A.7). Figure A.9 indicates dissolution of the hematite matrix such that the electrode does not adequately conduct current.

As pH increases, the peak area decreases (Table 5.1). At pH 5.5-10, uranium peaks are difficult to observe, which indicate that uranium redox reactions are either thermodynamically unfavorable or kinetically slow relative to the applied scan rate. At pH values between 4-5.5, the peak height of the uranium redox transformations is very small, yet definable. Since the same scan rate was used in all experiments, higher peak

area can be associated with more material oxidized (or reduced in the case of a cathodic peak), which is a result of faster kinetics and more favorable redox conditions.

Table 5.1. Summary of CV peak parameters and uranyl speciation at varying pH. Uranium values are given as percentage of total uranium. The peak area could not be quantified because the baseline for the peak could not be clearly defined Additional CV data at varying pH is given in Figures A.8 – A.13.

pH	Potential	UO_2^{2+}(%)	$UO2(SO4)_2^{2-}$(%)	$UO_{2x}OH_{y+}$(%)	$(UO_2)SO_4$(%)
3	0.13	9.68	26.4	0.02	63.9
3.79	0.18	9.58	26.5	0.23	63.7
4.09	0.22	9.52	26.5	0.58	63.4
5.15	0.2	4.95	14.1	47.6	33.3
6.27	0.2	0.09	0.25	99.1	0.58

Table 5.1 indicates an increase in peak potential with higher pH up to approximately pH 4.   Above this pH the potential equilibrated to about 0.2V. Above pH 6.5 the anodic peak resolution was too poor for reliable quantification. A change in uranyl speciation, modelled using Visual Minteq, from free uranyl/uranyl sulphates to uranyl hydroxide species is observed at pH 5.15. Total peak area also decreases at this pH, which may be due in part to the change in speciation. More definitive conclusions cannot be reached until the chemical environment of incorporated U(VI) and U(IV) during the redox reactions is better characterized.

In summary, the total peak area generated during a uranium redox event varies with pH. Peak area was greatest at pH ~3.5, while iron redox was significant at pH >10. Uranium redox is not observable above pH 5.5 using this analytical technique. Below a pH of ~3, the hematite electrode begins to dissolve inhibiting the use of the PME for probing uranium redox reactions.

Characterization of Uranium Redox with Varying Temperature

Temperature, as shown by the Nernst equation (Equation 1), directly affects the electrochemical potential of a redox reaction. The Arrhenius equation dictates that reaction rate constants also increase with increasing temperature:

$$k = A * e^{\wedge}(-\frac{E_a}{RT}) \tag{5}$$

Where k is the rate constant, E_a is the activation energy of the reaction, A is a constant, and T is the temperature. As a result, temperature will change the extent of the reaction during a CV experiment, thereby changing the total number of electrons transferred. Peak area will change as a result. To evaluate the effect of temperature on redox reactions of U-doped hematite, a series of CV scans were collected for an electrochemical cell immersed in a water bath (or ice bath for below room temperature measurements). (Figure A.14). Figure 5.11 shows the peak area of the U(IV) anodic CV peak as a function of temperature.
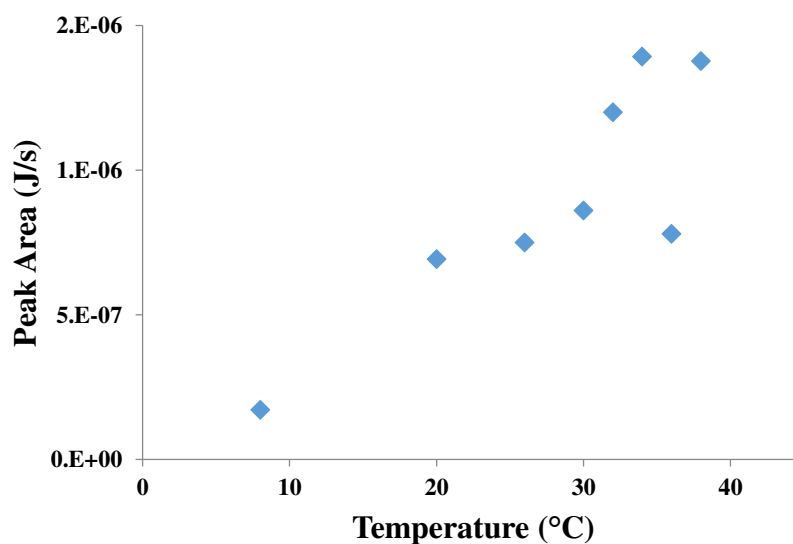
Figure 5.11. Summary of peak areas measured at changing temperature. Original CV data shown in Figures A.15-A.21.

The cathodic and anodic peak potential is a thermodynamic property of a given reaction

with consideration of the reaction environment (*e.g.*, the anodic peak potential for Fe(II)

to Fe(III) oxidation in aqueous solution at pH 7 is 0.771 V)[25]. However, some material is

oxidized/reduced at a slower rate as the applied voltage approaches the cathodic/anodic

peak potential. A shift in the peak onset potential indicates a change in the kinetics of the

redox reaction. That is, faster oxidation kinetics causes more material to be oxidized

more readily during the CV experiment, leading to an earlier onset for the anodic peak as

indicated by a shift to lower voltages. Table 5.2 further illustrates this point showing that

the peak onset shifts to lower voltages as temperature increases

Table 5.2. Summary of CV peak potential, peak area, FWHM, and peak onset of anodic U(IV) peak at varying temperature. The designation 'ND' indicates that the indicated parameter could not be determined. CV data at varying temperatures is provided in Figures A.15 – A.21.

Temperature	Peak Potential (V)	Peak Area (J/s)	FWHM	Peak Onset (V)
8	0.196	5.02E-06	ND	0.071
20	0.186	5.58E-07	0.115	-0.013
26	0.175	6.86E-07	0.079	-0.027
30	0.133	8.32E-07	0.093	-0.045
32	0.165	1.14E-06	0.098	-0.076
34	0.144	1.29E-06	0.118	-0.087
36	0.154	7.28E-07	0.121	-0.065
38	0.123	1.38E-06	0.126	-0.091
45	ND	ND	0.251	ND
49	ND	ND	0.211	ND

 Figure 5.12 relates the anodic peak potential of the U(IV) to U(VI) oxidation reaction as

a function of temperature, showing that temperature may also change the peak potential

due to thermodynamic considerations. The anodic peak potential shifts to more negative

values with increasing temperature, which adds to the shift in the peak onset. However, the difference in onset potential and peak potential do not change at the same rate with increasing temperature. As a result, shifts in peak onset cannot be entirely attributed to a shift of the peak potential, and are in part due to faster reaction kinetics. Free energy depends on reaction enthalpy and entropy as shown by the following relationship:

$$\Delta G = \Delta H - T\Delta S \tag{6}$$

The apparent decrease in reaction free energy may be due to entropic costs associated with oxidation of incorporated U(IV) to U(VI). Further evaluation of entropic effects will require rigorous computational modeling and structural analysis. Ilton et. al. (2012) indicated that incorporated U(IV) is more stable with a higher coordination number relative to U(VI). Oxidation of incorporated U(IV) may entail breaking chemical bonds and, in turn, a corresponding enthalpic cost, which decreases the reaction free energy.
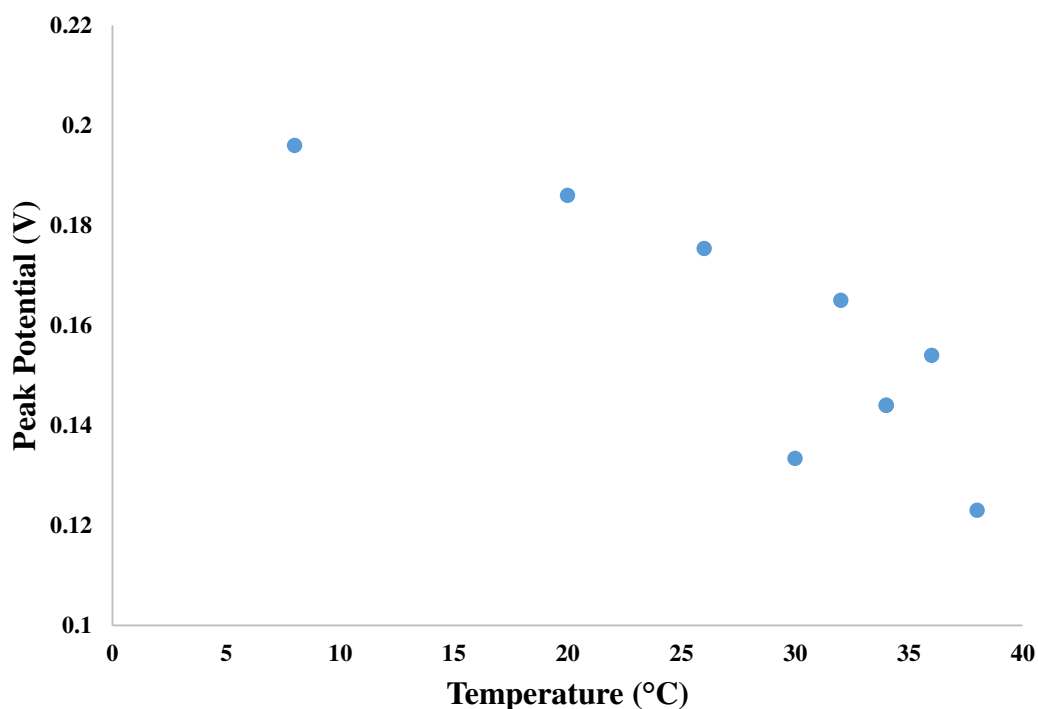
Figure 5.12. Peak potential of U(IV) as a function of temperature.

The preceding discussion is applicable to temperatures up to ~34°C, at which point the U(IV) oxidation peak begins to broaden. With higher temperature, additional noise in the system increases the baseline of the CV scan. This factor, combined with additional peak broadening, causes the peak to become indistinguishable from the baseline above 50 degrees (See Figure A.22). Figure 5.13 demonstrates that the full width at half maximum (FWHM) of the U(IV) oxidation peak begins to increase at 35 degrees, with a sharp increase at 45 degrees corresponding to the broadening of the peak and the increase of the baseline. As the peak broadens and becomes less well defined, measurement of peak area becomes more difficult and is a less suitable kinetic indicator. As a result, CV is not a reliable method for investigation of uranium redox at elevated temperatures
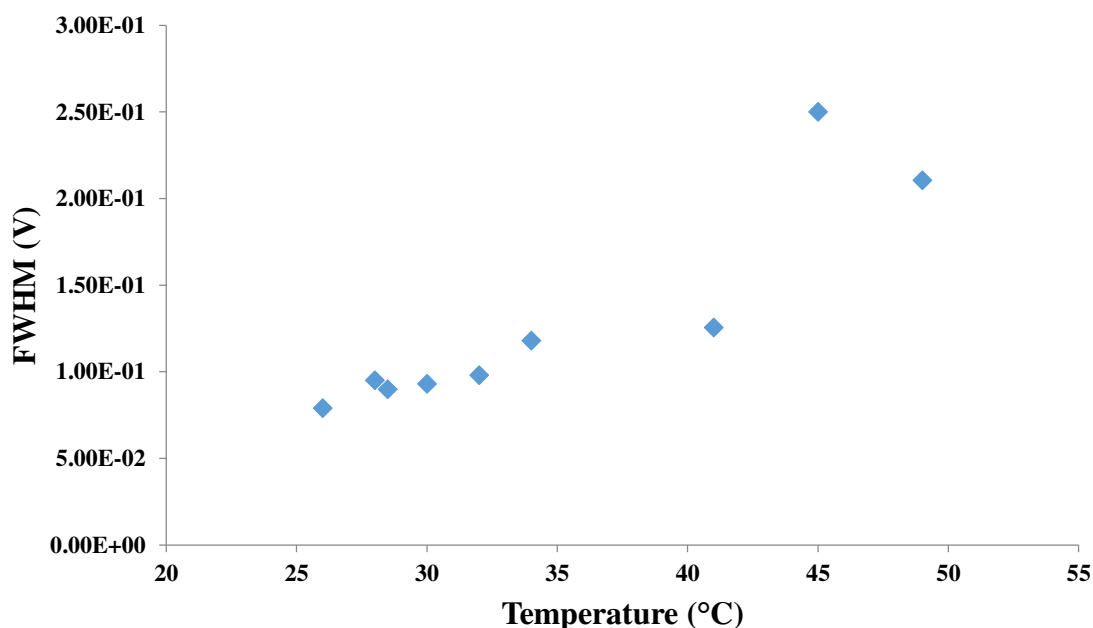
Figure 5.13. FWHM of U(IV)/(VI) oxidation peaks during first cycle of CV scan.

In summary, uranium redox processes are kinetically enhanced by increasing temperature up to 35 °C. Above this temperature the U(V) and U(VI) reversible couple becomes more difficult to observe. Above 50 °C no uranium redox is observed. Experimental measurement of uranium redox with increasing temperature is limited by an increase in the background current.

Effect of Hematite Aging on Doped-Uranium Redox

Amorphous iron oxide requires a period of thermal incubation to age the hematite structure and incorporate uranium[39]. Uranium incorporation into hematite is expected to occur via substitution into an octahedral site. The extent of uranium incorporation into hematite is dependent on the crystallinity of the sample, particularly the ordering of the octahedral sites. To assess the effect of aging on uranium redox processes, uranium-

doped hematite samples were synthesized and aged for 3, 7, 14, and 28 days prior to CV experiments. The samples were evaluated using powder XRD, as shown in Figure 5.14.
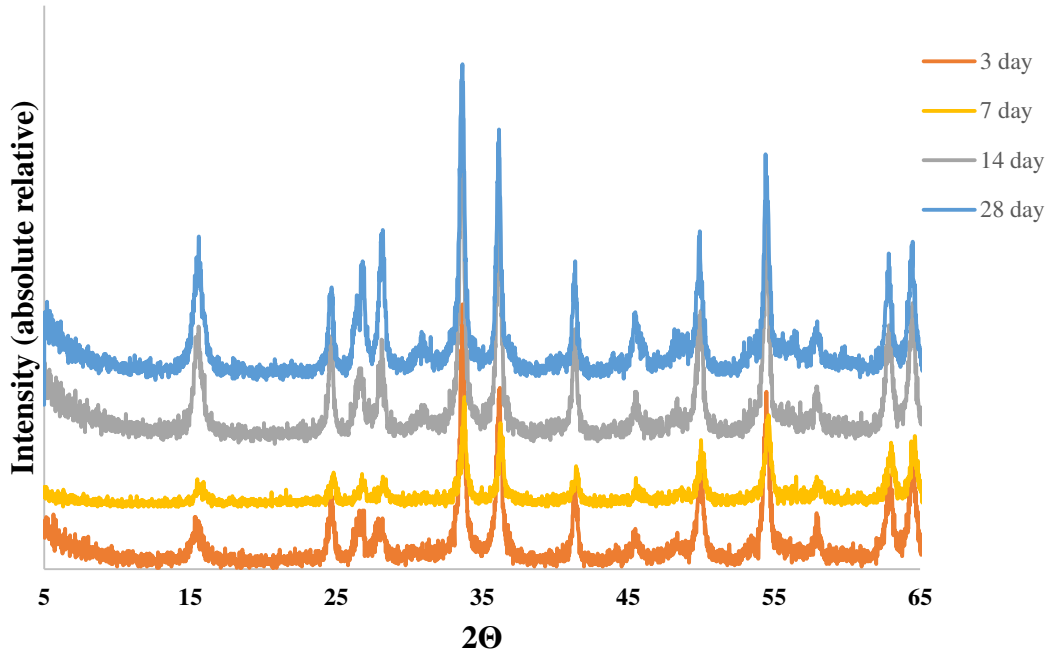
Figure 5.14. XRD spectra of uranium-doped hematite synthesized and incubated for 3, 7, 14, and 28 days.

The peak intensity is, in part, a function of the degree of crystallinity of the sample. However, experimental factors may also change relative intensity. These factors can be de-convoluted through the use of an internal standard sample of known crystallinity. In the absence of an internal standard, extreme caution should be made when evaluating peak intensity between two samples of a common mineral. The absence of an observed correlation between peak intensity and incubation time in Figure 5.14 indicates that sample quantity and/or orientation was the most significant determining factor in observed intensity. As can be seen in Figure 5.14, the XRD spectra for each of the samples overlay each other with minimal deviations in peak width and location. As

crystallinity increases, the resolution of the XRD peaks should increase as well. The absence of an observable increase in peak resolution with increasing incubation time strongly indicates that the samples approach full crystallinity at three days.

However, ICP-MS results from the supernatant of the wash cycles of each sample indicates that aging has an effect on the amount of uranium irreversibly associated (sorbed or incorporated) with the hematite (Figure 5.15). As described previously, the first five washes were conducted with a carbonate solution, and the last five were conducted with DI water. For the 3 day sample, 5.2 atomic % of uranium was removed during washing, whereas for the 28 day sample 1.1 atomic % of uranium was removed. As a result, samples aged for longer periods demonstrated a higher percentage of uranium permanently associated with the mineral. This difference may be indicative of higher amounts of incorporated uranium, or lower rates of uranium desorption. In the former scenario, longer incubation periods may allow the hematite structure to age such that incorporated uranium is stabilized in a less distorted octahedral sites. Marshall et. al. (2014) found that uranium was incorporated into hematite during ferrihydrite precipitation and the initial formation of hematite crystals. However, as the mineral continued to age, additional uranium incorporation was observed. Previous work has also demonstrated the tendency for actinide desorption rates to decrease as a function of time due to aging of the mineral surface[40]. Thus, adsorbed uranium may simply be more difficult to remove from aged hematite. In this case, the difference in fixed uranium between the 3 and 28 day sample (94.2% versus 98.9%) is, at least in part, attributable to higher uranium desorption from the 3 day sample.
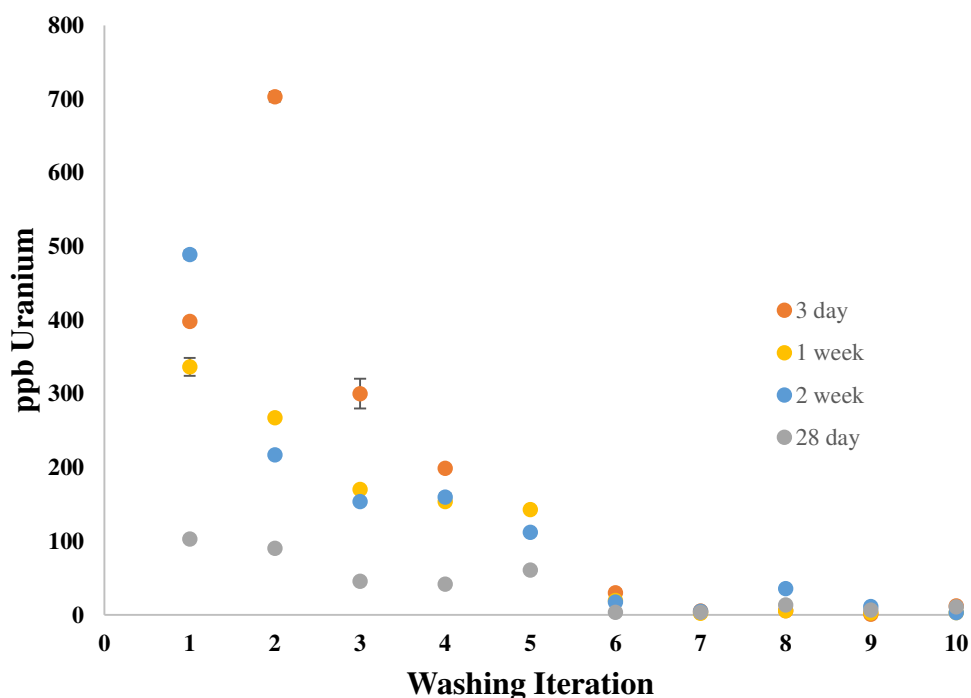
Figure 5.15. Uranium removed from doped hematite at various incubation periods as a function of washing iteration. A carbonate wash was used for washing iteration 1-5 and a DI wash was used for washing iterations 6-10.

Additional insight can be obtained from the CV for the 3 day and 28 day aged samples (Figure 5.16). Additional data is included in Figure A.24. The peak potential (0.197 V and 0.207 V for the 3 day and 28 day samples, respectively) and peak onset (-0.045 V) for the U(IV) and U(V) oxidation peaks are similar for both CV scans, while the peak area of the 3 day sample (8.95 E-08 J/s) is more than twice that of the 28 day sample (3.43 E-08 J/s). This strongly indicates that higher quantities of uranium were oxidized in the 3 day sample relative to the 28 day sample. This observation provides support for the hypothesis that higher quantities of uranium are sorbed, rather than incorporated, in the 3 day sample relative to the 28 day sample. As described by Ilton et. al. (2012), incorporated U(VI) readily reduces to U(V), whereas sorbed U(VI) readily reduces to

U(IV). It must be remembered that CV supplies a constant source of electrons that can force the reduction of incorporated uranium to U(IV). Nevertheless, during voltage pre-conditioning sorbed U(VI) should more readily reduce to U(IV). The current generated during the subsequent oxidation of U(IV) is in turn dependent on the initial population of U(IV). Thus, sorbed uranium should generate higher current during the oxidation of U(IV) to U(VI).
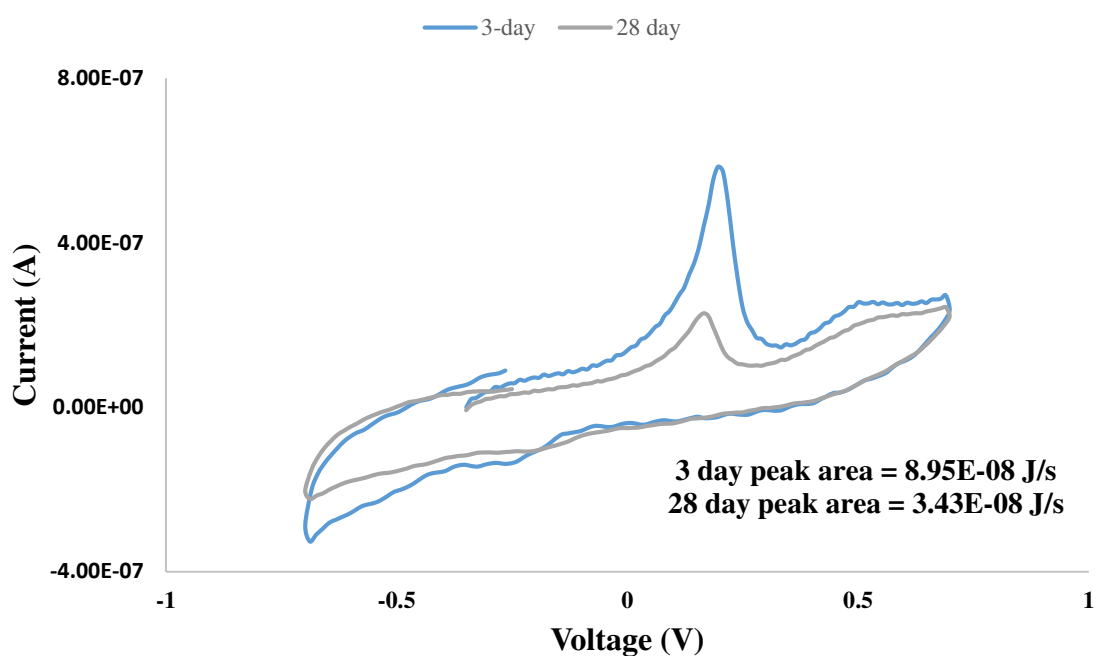
Figure 5.16. CV spectra of uranium doped hematite synthesized at varying incubation times.

In summary, hematite samples were not found to exhibit increasing crystallinity as a function of incubation time, as confirmed by XRD analysis. The fraction of removable uranium decreased as with incubation time, as measured by ICP-MS, showing that aging did affect the amount of U irreversibly associated with the synthesized hematite. The relative peak area for the U(IV) to U(VI) oxidation was much larger for

the 3-day sample (8.95E-08 J/s) compared to the 28-day sample (3.43E-08 J/s). This

indicates that more uranium was available for oxidation.

CHAPTER SIX

Closing Remarks

Conclusions

The preliminary objective of this work was to synthesize hematite containing incorporated uranium. Rigorously demonstrating that U is incorporated into the synthesized hematite is difficult; however, experimental results give a strong indication that at least a portion of the uranium is permanently associated with hematite and likely incorporated. ICP-MS shows that ~99% of the uranium used in the initial synthesis remains associated with the doped hematite system after extensive washing. XRD analysis of the doped sample indicates a slight shift in the spectra, which is indicates a reduction in the lattice parameters of the mineral. Incorporation of uranium into the mineral must leave Fe(III) vacancies, which may cause an overall constriction in the lattice parameters and cause the observed XRD shift. Future computational work is necessary to verify this prediction.

XRD analysis also showed additional peaks on the doped hematite samples that may be attributable to the mineral clarkeite. Clarkeite and hematite are very similar crystallographically, both belonging to the *R3* space group. Therefore, one might expect nearly identical diffraction patterns TEM analysis of the doped hematite indicated that the mineral was morphologically homogeneous. The inability to locate a secondary uranium phase may indicate that the XRD peaks attributed to clarkeite are in fact caused by structural alteration to hematite caused by uranium incorporation.

The second objective of this work was to investigate if the uranium doped hematite system undergoes electrochemical changes. As measured by CV, U(VI) was reduced to U(IV) upon the application of a pre-conditioning voltage. U(IV) was then re-oxidized to U(VI) during the initial positive voltage sweep. U(VI) was reversibly reduced to U(V) on subsequent voltage cycles. Ilton et al (2012) proposed that U(V) is more stable in an octahedral coordination environment than U(VI), which naturally favors reduction to U(V) for incorporated uranium. Ilton found that U(VI) reduction to U(IV) was preferred for non-incorporated uranium on the surface of the mineral. U(IV) in our experiments may thus be indicative of a significant population of uranium on the surface. However, due to the application of external energy in our system, the thermodynamic limitations that restrict the formation of U(IV) in Ilton's work may not be evident. However, it must be remembered that a variety of convoluting factors, such as voltage scan rate, affects the system and complicates direct comparison between CV experimental results and other literature findings.

The electrochemical properties of uranium in the doped hematite system were shown to be strongly affected by external physical parameters. Uranium redox transformations were found to be highly pH dependent and most strongly observed within a narrow pH range centered about pH 3.5. The uranium redox peaks likely contain contributions from both incorporated uranium and sorbed uranium, although the relative contribution of each component remains uncharacterized. The contribution of sorbed and incorporated uranium to total current may not necessarily be directly proportional to the distribution of total uranium in the system. As a result, enhanced current at low pH may

be due to higher desorption of uranium and/or liberation of structural uranium from partial dissolution along grain boundaries.

Uranium redox demonstrated a dependence on temperature, particularly below ~34 °C. Total peak current increased as a function of temperature up to ~34 °C, which is indicative of increased kinetics. Above this temperature, the combination of an elevated baseline and peak broadening caused the uranium redox peaks to become unobservable. Given the limitations of the CV technique at higher temperatures, alternative experimental methods are required to more fully probe these effects at higher temperatures.

The crystallinity of the doped hematite did not significantly vary with incubation time. ICP-MS analysis indicated a trend between incubation time and total uranium removed from the surface of the sample after washing. These results may be attributed to less uranium desorption with longer incubation time. Alternatively, they may be indicative of greater incorporation efficiency due to aging of the hematite structure.

The summation of the experimental results indicate the following:

(1. The majority of uranium in the doped hematite sample is permanently associated with the hematite as either a co-precipitated phase, irreversibly sorbed uranium, or incorporated uranium.

(2. Uranium in the doped hematite system undergoes electrochemical transformation in the presence of an induced voltage. Given the analytical results regarding the association of uranium in doped hematite, it is likely that the observed uranium electrochemistry is due in part to uranium incorporated into hematite.

56

(3. Physical parameters, such as pH and temperature, affect the rate of uranium

redox; for example, uranium redox is observable only at specific pH values.

Future Work

The combined evidence of XRD, SEM/EDS, TEM, and ICP-MS strongly

indicates that uranium is incorporated into the hematite sample, but does not reveal the

local coordination environment of the U associated with the synthesized hematite. Future

experimental work would benefit from X-ray Absorption Near Edge Structure (XANES)

spectroscopic analysis of the doped hematite, which could be used to determine the

coordination environment of the uranium and bond lengths within the mineral. An

understanding of the microscopic structure of the uranium coordination environment

would allow the incorporation mechanism and stability of the coordinated uranium to be

better understood.

The redox reactions of uranium incorporated into a range of proximal minerals at

a given disposal site is of significant importance for risk assessment of radioactive waste

disposal sites. Therefore, this work should be expanded to study additional iron oxide

minerals, such as magnetite and goethite. Uranium sorption reactions on these minerals

are similar to those observed on hematite[25]. Similarities and differences in uranium redox

between iron oxide minerals could therefore provide valuable information on the role of

the coordination environment on uranium redox processes. Finally, computational

modelling is necessary to provide greater insight into the thermodynamic stability of

incorporated uranium. For example, the stability of U(VI) in the octahedral hematite

environment is an important issue that cannot be addressed solely with experimental data.

REFERENCES

(1) *Comparison of Lifecycle Greenhouse Gas Emissions of Various Electricity Generation Sources.* World Nuclear Association, **2011**

(2) Fetter, S. How Long Will the World's Uranium Supplies Last? *Scientific American.* Jan. 26, 2009.

(3) Johnson, L.; Ferry, C.; Poinssot, C; Lovera, P. *Journal of Nuclear Materials* **2005,** *346,* 56-65.

(4) Buck, E.; Hanson, B.; McNamara, B. The geochemical behavior of Tc Np and Pu in spent nuclear fuel in an oxidizing environment. In *The Geological Society of London Special Publication.* **2004,** *236,* 56-88

(5) Wronkiewicz, D.; Buck, E. *Mineralogical Society of America Reviews in Mineralogy.* **1999,** *38,* 475-497.

(6) Bruno, J.; Ewing, R. *Elements* **2006,** *2,* 343-349.

(7) Flanagan, S.; *Natural Chemistry of Shallow Groundwater,* United States Geological Survey publications, **2005.**

(8) Poinssot C.; Ferry C.; Lovera P.; Jégou C.; Gras J-M. *Journal of NuclearMaterials* **2005,** *346,* 66-77.

(9) Choppin, G.; Jensen, M. Actinides in Solution: Complexation and Kinetics. In *The Chemistry of the Actinide and Transactinde Elements,* 4th ed.; Morss, L. R., Edelstein, N. M., Fuger, J., Eds.; Springer: Dordrecht, The Netherlands, 2008; pp 2524-2621.

(10) Regenspurg, S.; Schild, D.; Schafer, T.; Huber.; Malmstrom, M. *Applied Geochemistry* **2009,** *24,* 1617-1625.

(11) Kersting, A.; Efurd, D.; Dinnegan, D.;. *Nature.* **1999,** 56-59.

(12) Novikov, A.; Kalmykov, S.; Utsonomiya, S.; *Science.* **2006,** 638-641.

(13) Stewart, B.; Nico, P.; Fendorf, S. *Environ. Sci. Technol.* **2009,** *43,* 4922-4927.

(14) Burns, P.; Ewing, R.; Hawthorne, F. *The Canadian Mineralogist* **1997,** *35,*1551-1570.

(15) Burns, P. *The Canadian Mineralogist* **2005,** *43,* 1839-1894.

(16) Ferriss, D.; Helean, K.; Bryan, C.; *Journal of Nuclear Materials.* **2009,** 130-139.

(17) Pauling, L.; Hendricks, S. *J. Am. Chem. Soc.* **1925,** *47,* 781-790.

(18) Maher, K.; Bargar, J.; Brown, G. *Inorganic Chemistry* **2013,** *52,* 3510-3532.

(19) Marshall, T. et. al.; *Environmental Science and Technology* **2014,** *48,* 3724-2731.

(20) Giammar, D.; Hering, J. *Environ. Sci. Technol.* **2001,** *35,* 3332-3337.

(21) Smith, S.; Douglas, M.; Moore, D.; Kukkadapu, R.; Arey, B. *Environ. Sci Technol.* **2009,** *43,* 2341-2347.

(22) Duff, M.; Coughlin, J.; Hunter, B. *Geochimica et. Cosomochimica Acta* **2002,** *66,* 3533-3547

(23) Ilton, E.S.; Pacheco, J.; Bargar, J.; Shi, Z.; Liu, J.; Kovarik, L.; Engelhard, M.; Felmy, A. *Environmental Science and Technology* **2012,** *46,* 2498-2436.

(24) Skomurski, F.; Ilton, E.; Engelhard, M.; Arey, B.; Rosso, K. *Geochimica et. Cosmochimica Acta* **2011,** *75,* 7277-7290.

(25) Bard, A.; Faulkner, F. (2001) *Electrochemical Methods.* Hoboken, NJ: Wiley and Sons.

(26) Ekstrom, A; *Inorganic Chemistry.* **1974,** *13,* 2237-2241

(27) Santos, B.; Noel, J.; Shoesmith, D. *Journal of Electroanalytical Chemistry* **2005,** *586,* 1-11.

(28) Hamilton, I.; Woods, R.; *J. Electroanal. Chem.* **1981,** *118,* 327-343(29)

(29) Nicholson R.; *J. Electroanal. Chem.* **1965,** *37,* 1351-1355

(30) Khan, A.; Ahmed, R.; Mirza, M.; *J. Chem. Soc. Pak.* **2008,** *30,* 170-177 CV hema

(31) Renock, D.; ueller, M.; Yuan, K.; Ewing, R.; Becker, U. *Geochimica et. Cosmochimica Acta* **2013,** *118,* 56-71.

(32) webmaster@ceb.cam.ac.uk: University of Cambridge Department of Chemical Engineering and Biotechnology Teaching Notes: Linear Sweep and Cyclic Voltammetry: The Basics. Cambridge, UK. 11/13/14

(33) Estes, S.; Powell, B. The Thermodynamic of U(VI) Sorption onto Hematite. In
      preparation for Geochimica et Cosmochimica Acta

(34) Cachet-Viver, C; Vivier V.; Cha, C.; Nedelic, N.; Yu, L. *Electrochimica Acta.* **2001,**

      47, 181-189
(35) Bond, A. *Analyst* **1994,** *119,* R1-R-20. PME

(36) Finch, R.; Ewing, R.; *American Mineralogist.* **1997,** *82,* 607-619

(37) Gorman-Lewis, D.; Burns, P.; Fein, J. *The Journal of Chemical Thermodynamics.*
      2008, *40,* 335-352

(38) Wang, Z.; Lee, S; Catalono, J.; *Environmental Science and Technology.* **2013,** *47,*
      850-858.

(39) Marshall, T. et. al.; *Environmental Science and Technology.* **2014,** *47,* 3724-3731

(40) Tinnacher, R.M.; Zavarin M.; Powell, B.; Kersting, A.; *Geochimica et*
      Cosmochimica Acta, **2011,** *75,* 6584-6599.

(41) Visual Minteq version 3.1, ***October 1, 2014.***
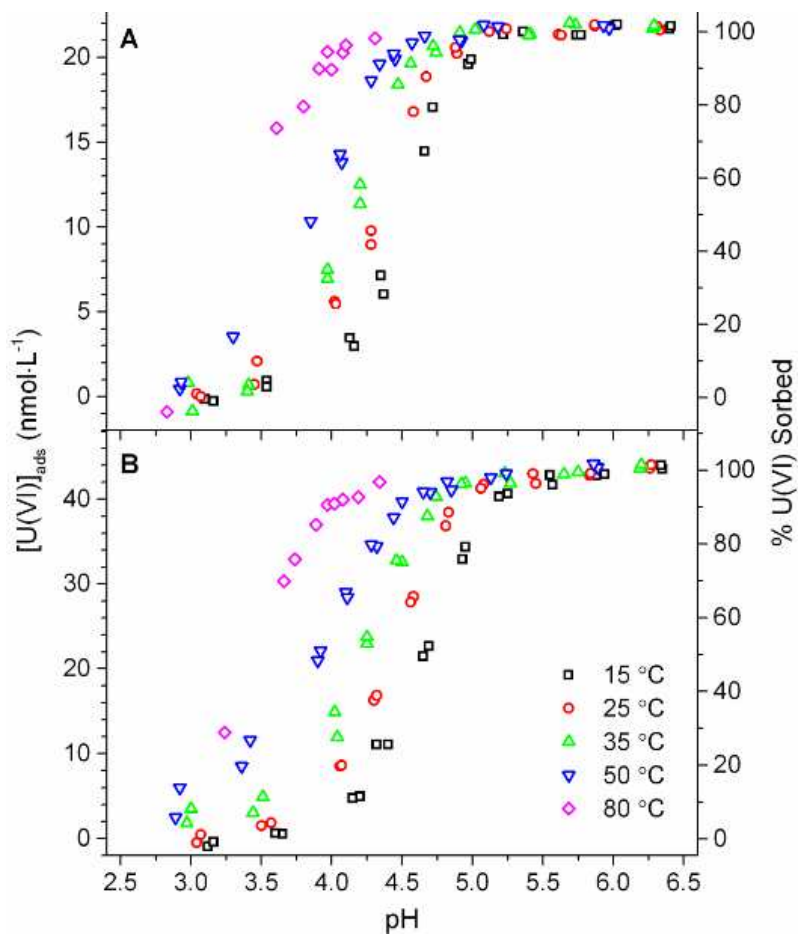
Figure A.1 Sorption of U(VI) on hematite surface as a function of pH and temperature[33]
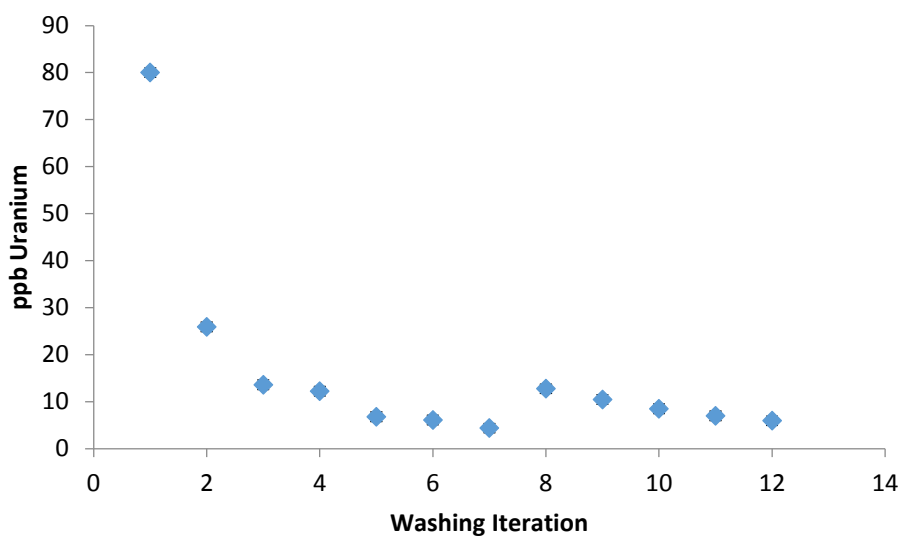
Figure A.2. ICP-MS analysis of uranium doped hematite after extended washing with .5M carbonate. Ten carbonate washes were conducted, with the final two wash sequences using DI water
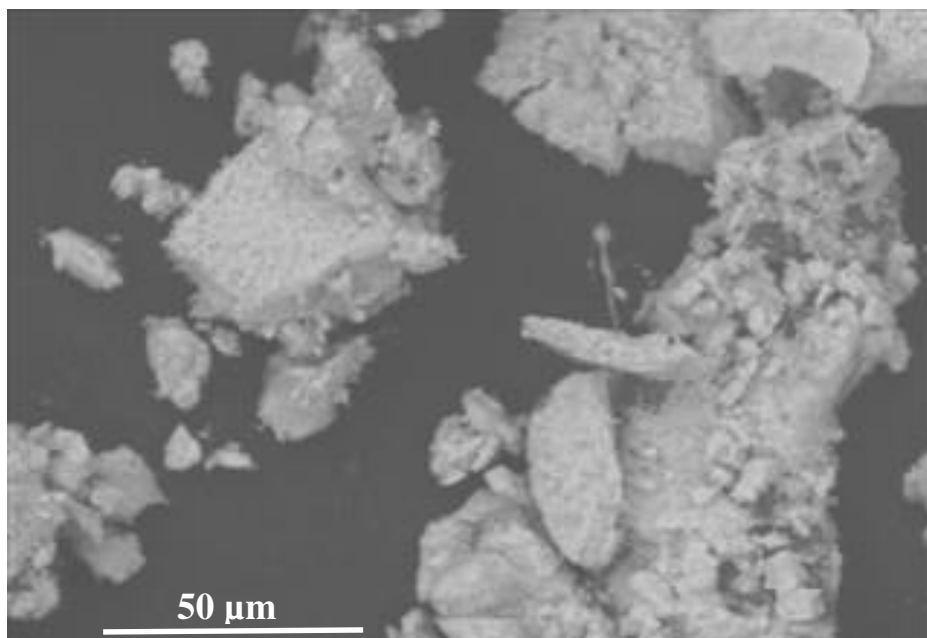
Figure A.3. SEM image of uranium doped hematite
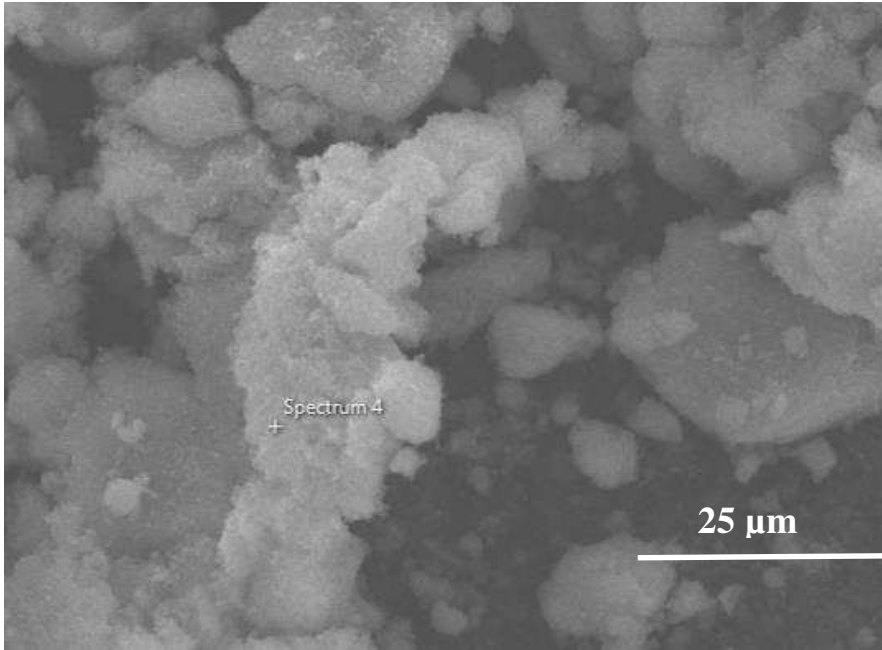
Figure A.4. SEM image of uranium doped hematite
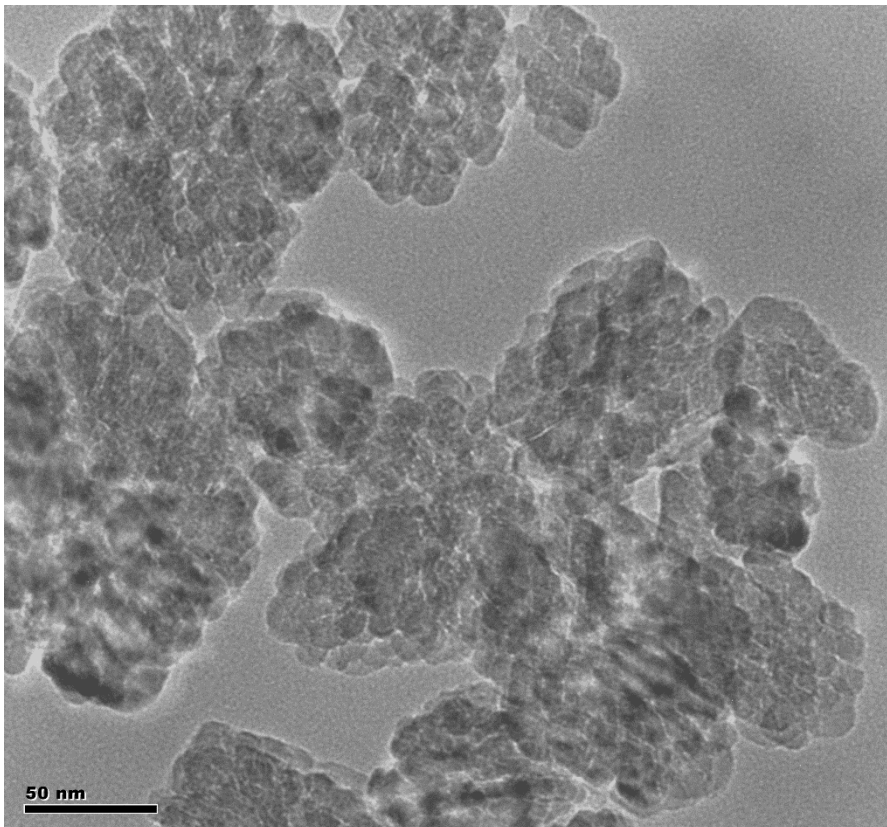
Figure A.5. TEM image of uranium doped hematite particles
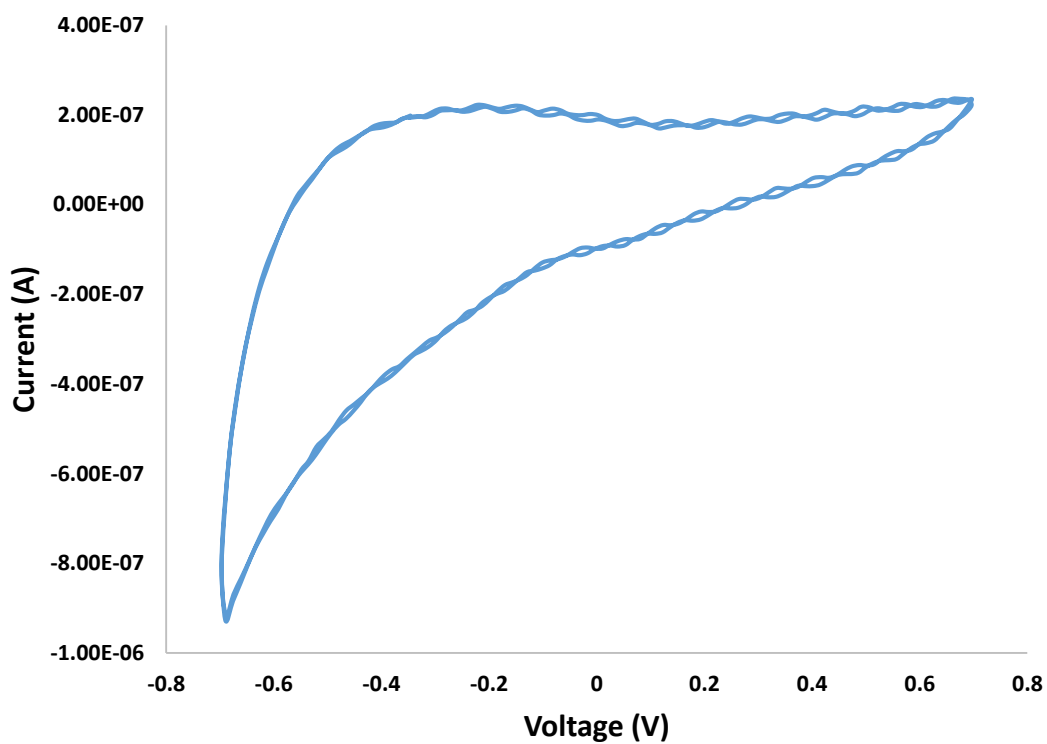
Figure A.6. CV scan of undoped hematite.
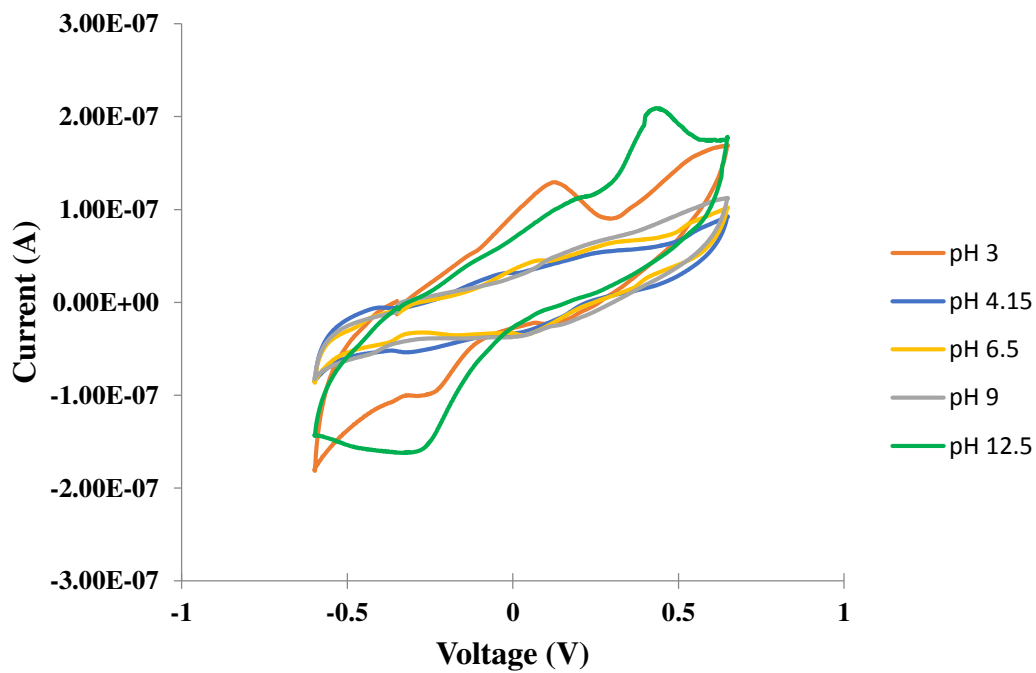
Figure A.7. CV data collected at varying pH
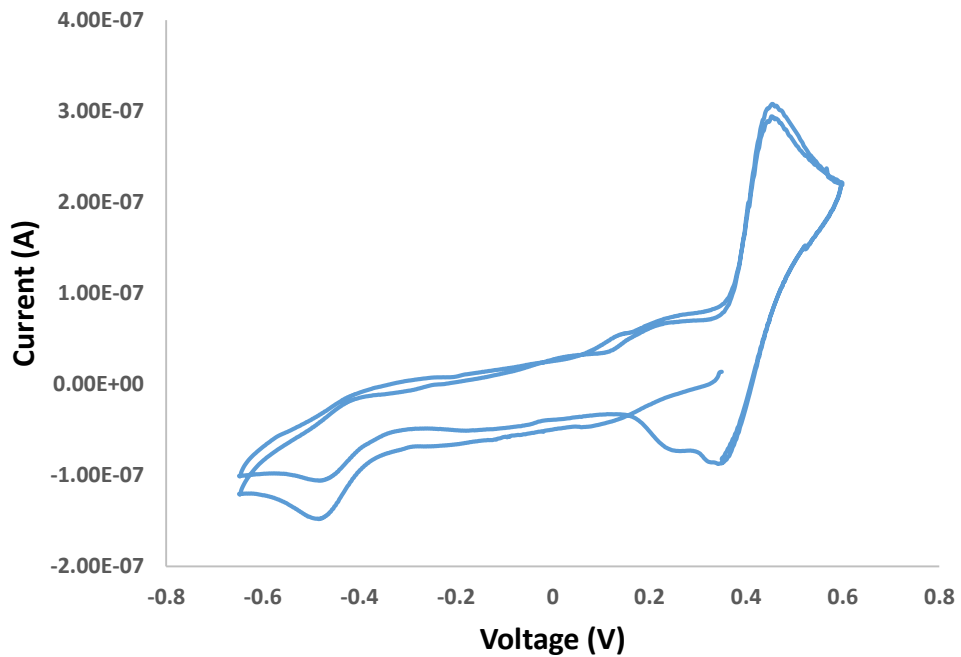
Figure A.8. CV spectrum of doped hematite at pH 2.9
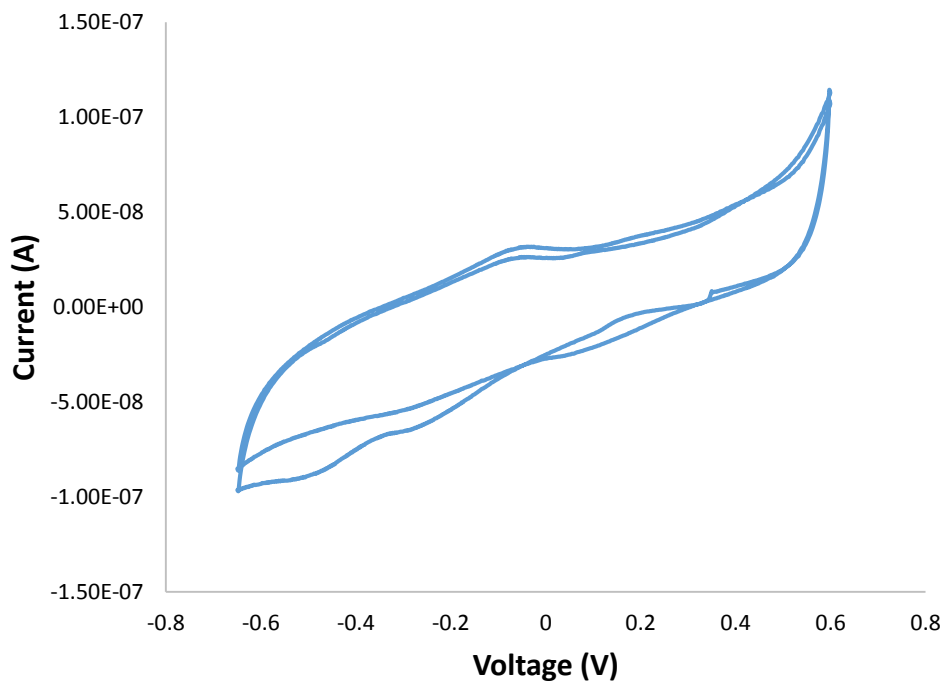
Figure A.9. CV spectrum of doped hematite at pH 4.91
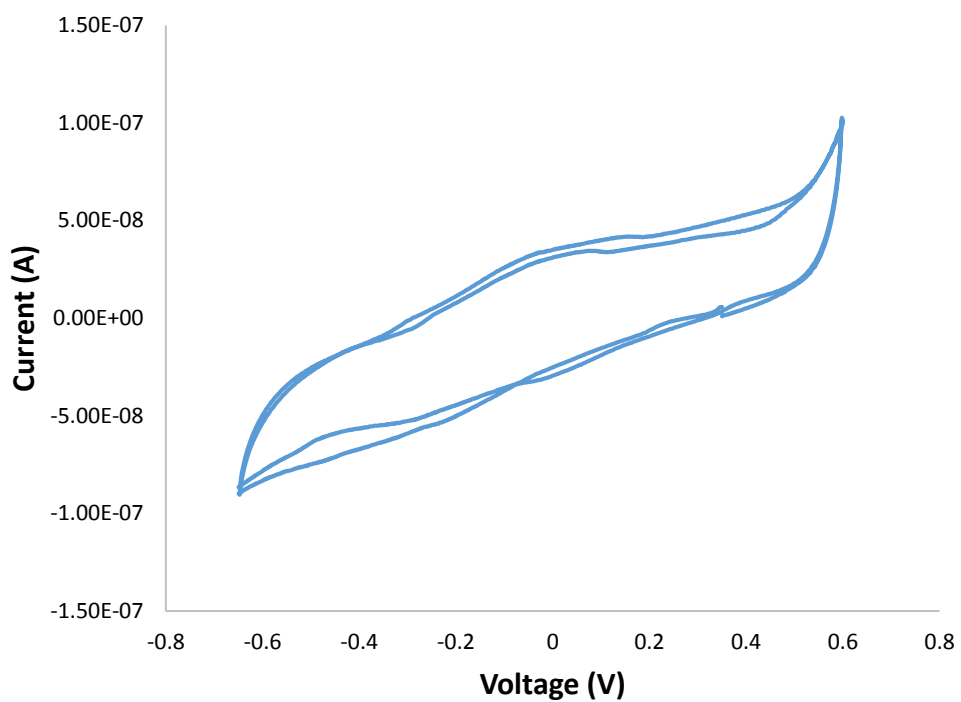
Figure A.10. CV spectrum of doped hematite at pH 6.27
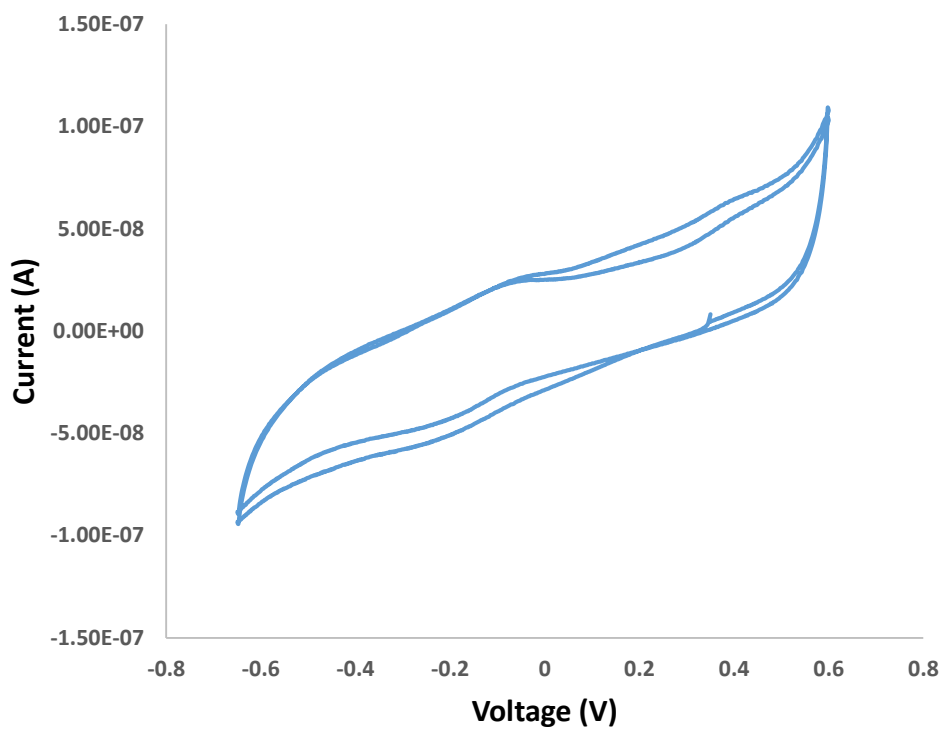
Figure A.11. CV spectrum of doped hematite at pH 7.67
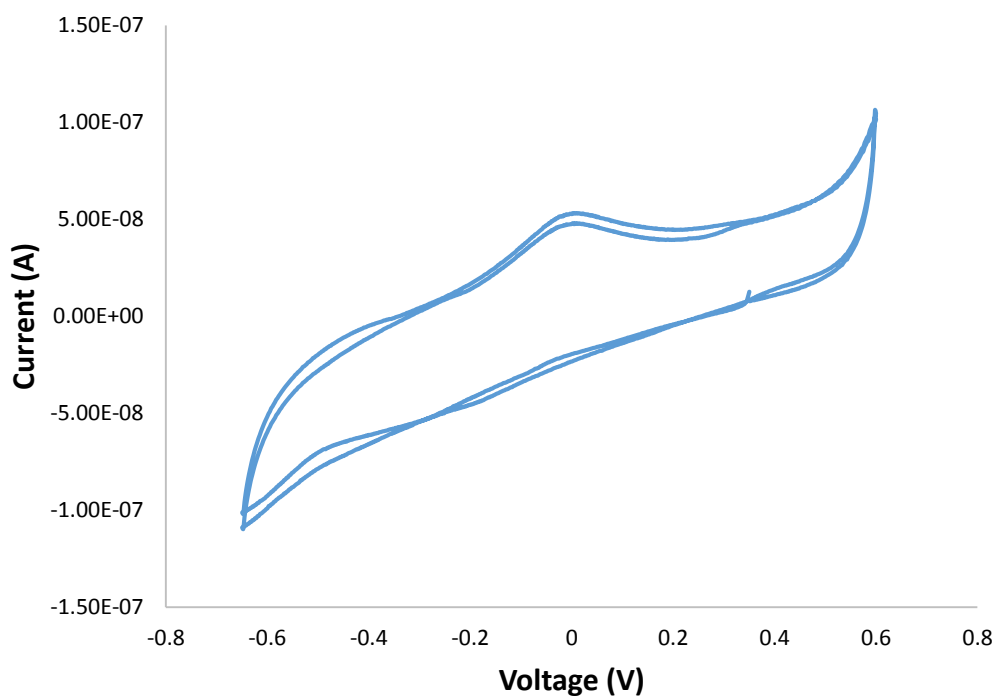
Figure A.12. CV spectrum of doped hematite at pH 10.27
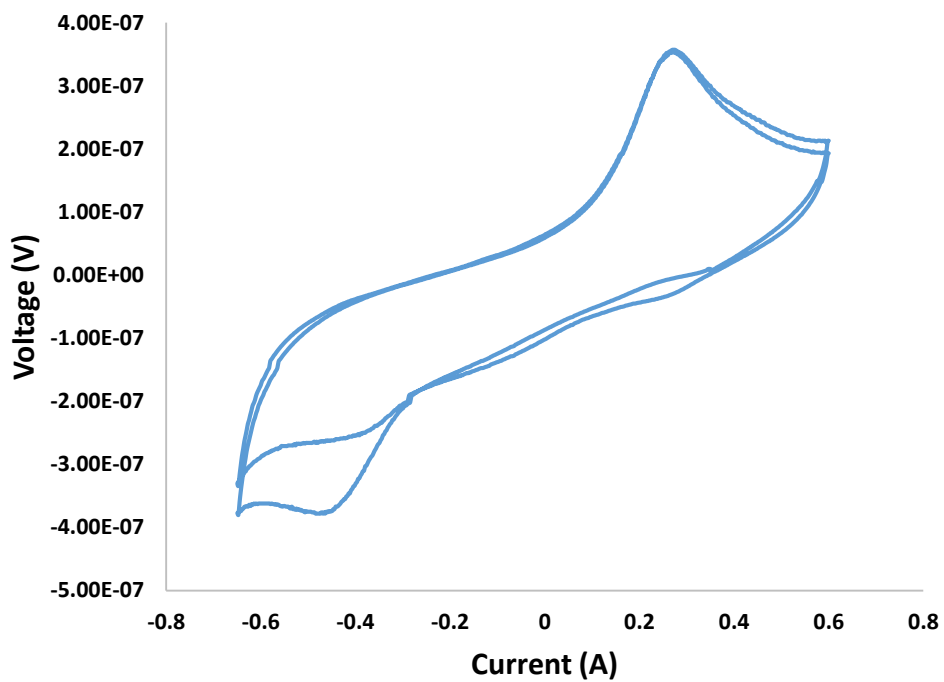
Figure A.13. CV of doped hematite at pH 13
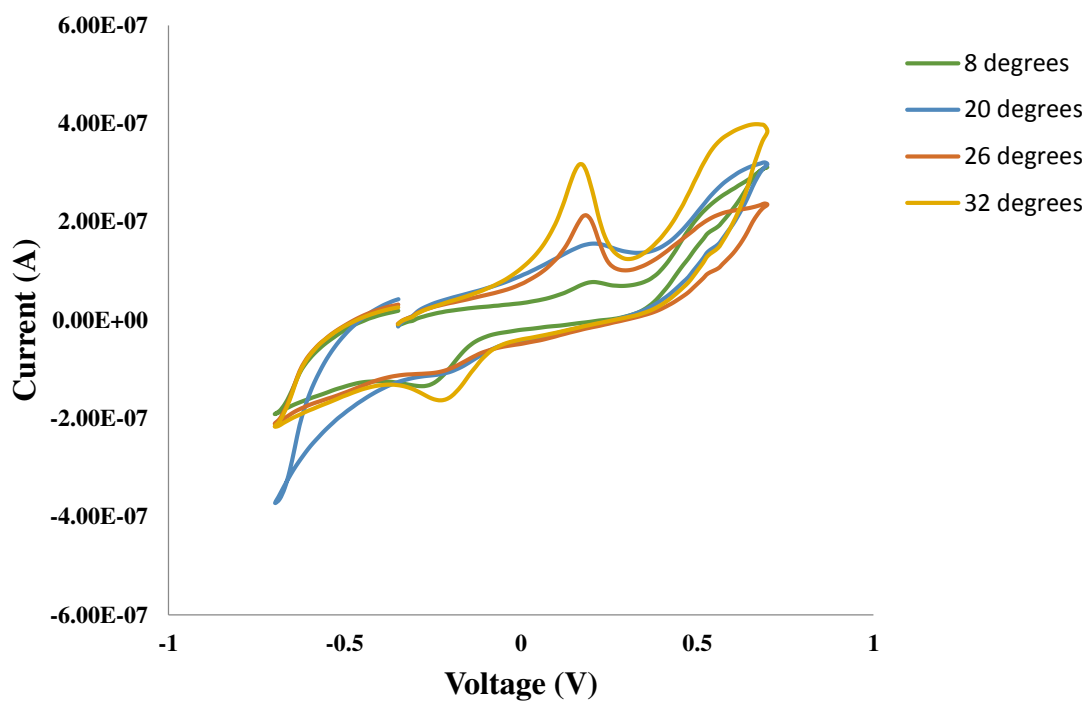
Figure A.14. Summary of CV data at varying temperature
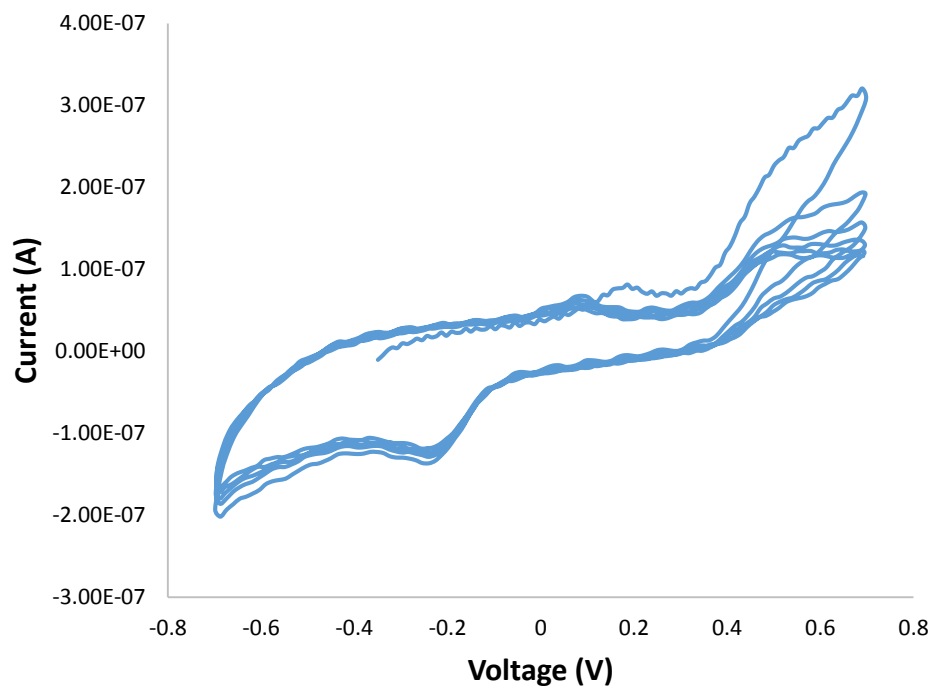
Figure A.15. CV scan of doped hematite at 6° C
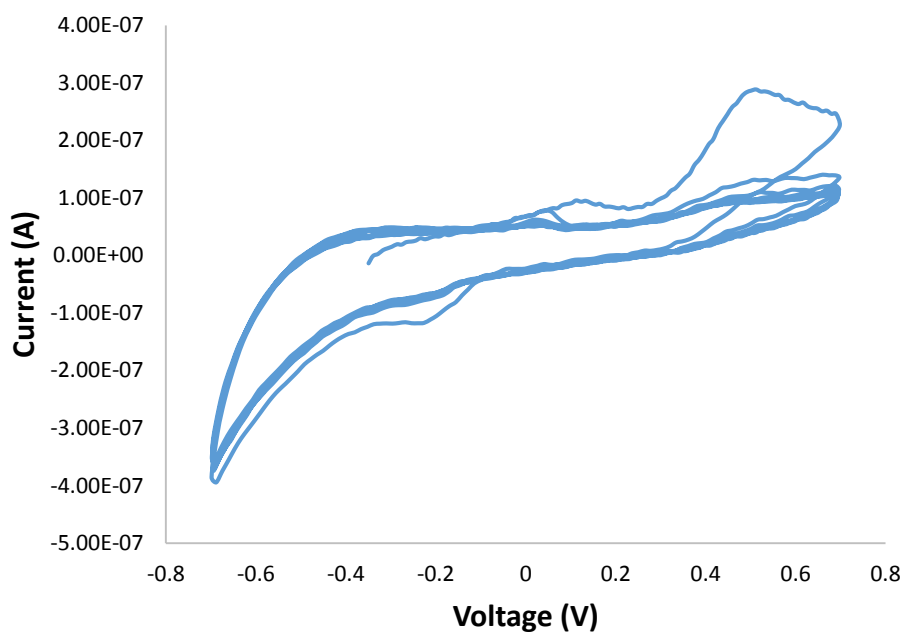
Figure A.16. CV scan of doped hematite at 18°
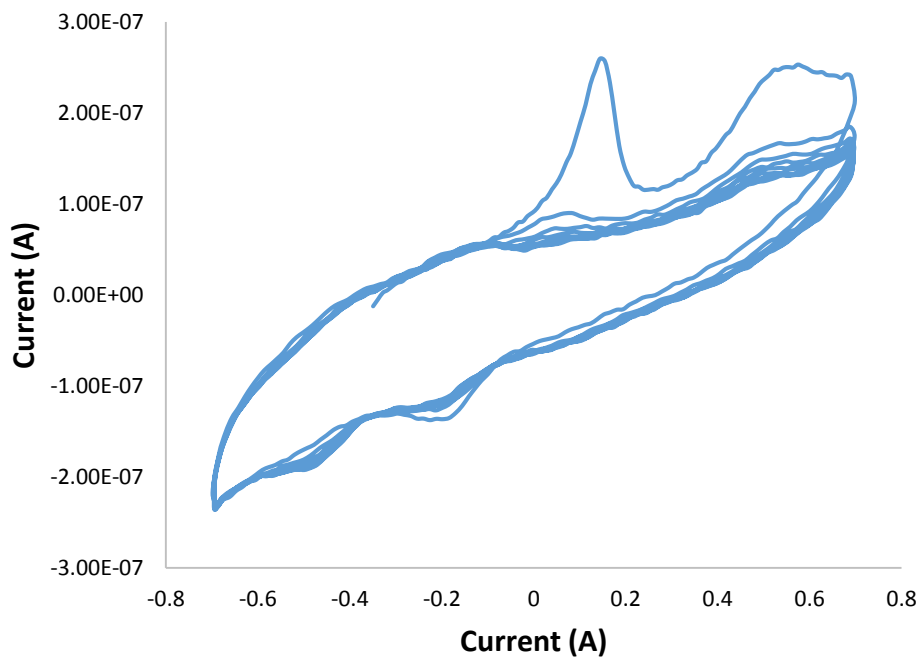
Figure A.17. CV scan of doped hematite at 26° C
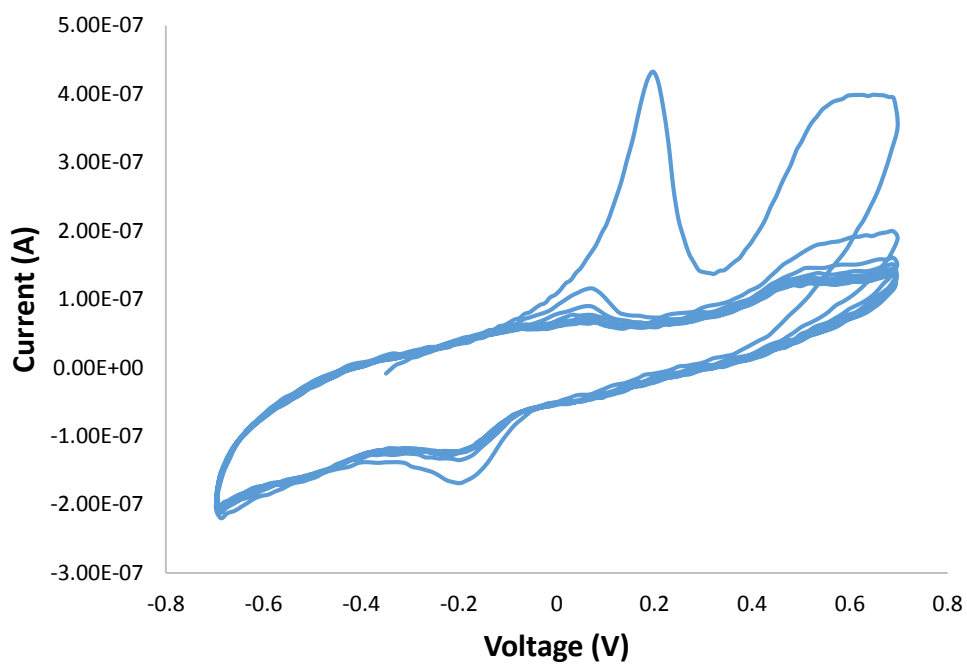
Figure A.18. CV scan of doped hematite at 28° C
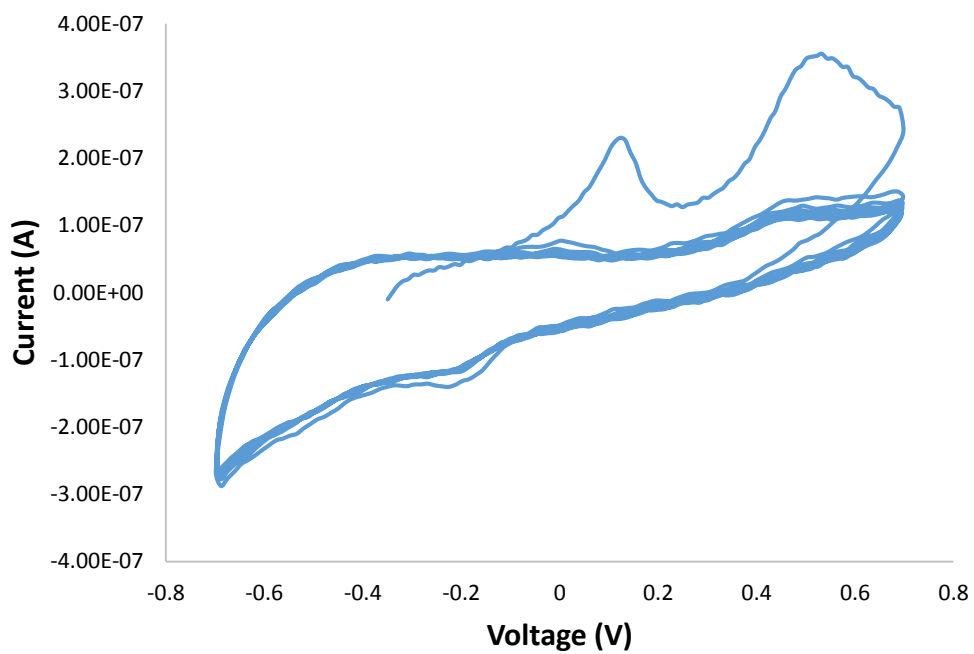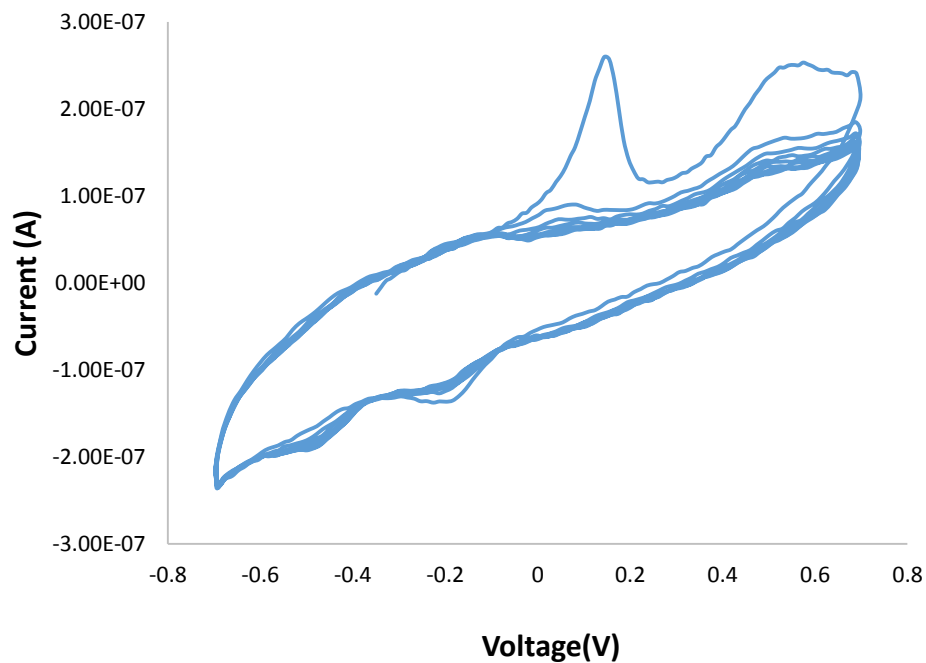

Figure A.19. CV scan of doped hematite at 30° C
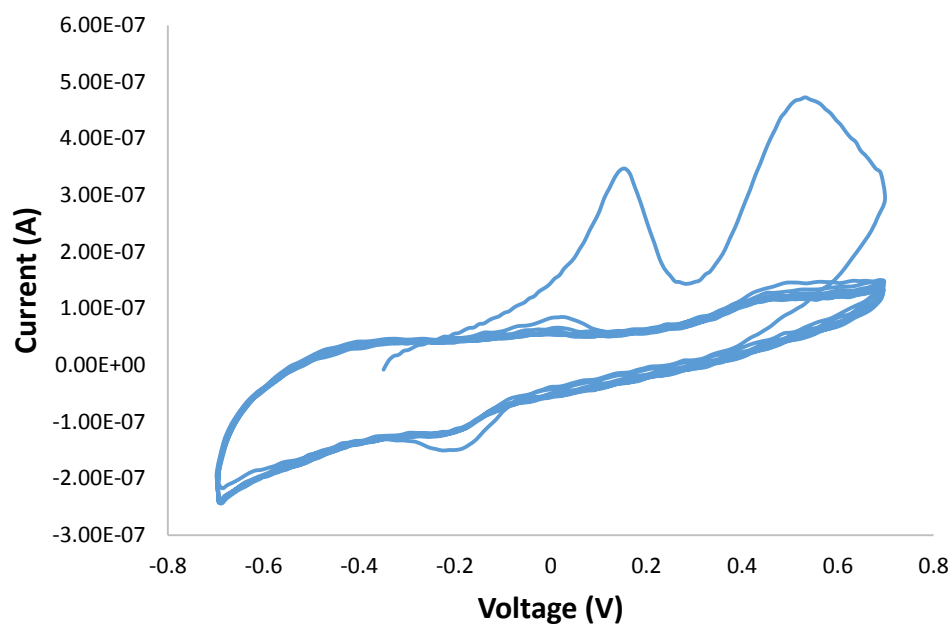
Figure A.20. CV scan of doped hematite at 34° C
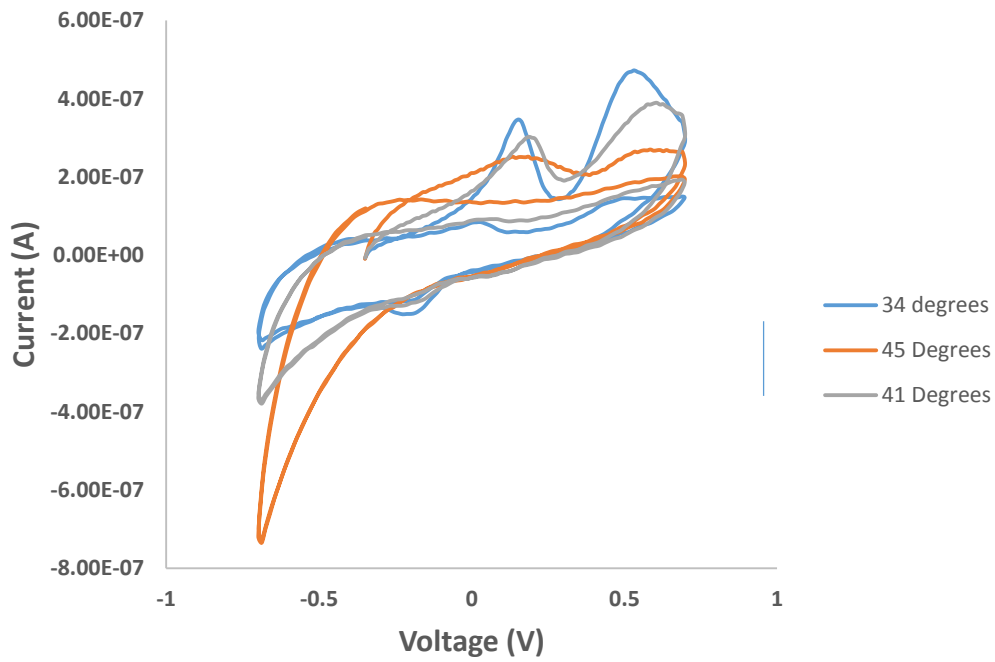

Figure A.21. CV scan of doped hematite at 36° C
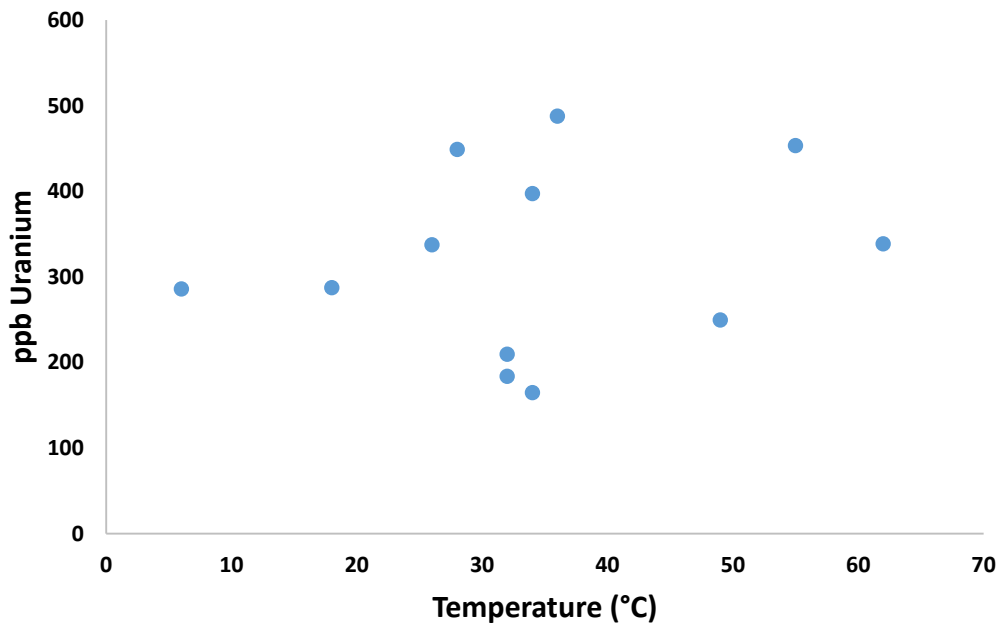
Figure A.22. Effect of temperatures above 34 °C.

Figure A.23. Uranium concentration in electrolyte solution following CV experiments at varying temperature.
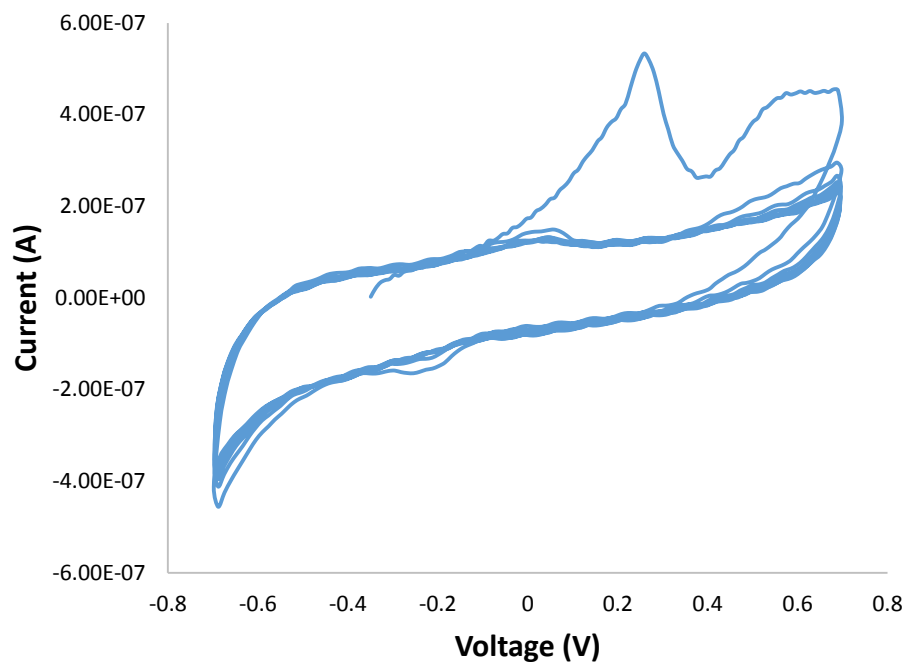
Figure A.24. Multi-cycle CV scan of doped hematite cycle incubated for two weeks